

**ISTANBUL TECHNICAL UNIVERSITY ★ GRADUATE SCHOOL OF SCIENCE**  
**ENGINEERING AND TECHNOLOGY**

**INVESTIGATION OF GRAPHENE/HOPG SYSTEM AND UHV  
SYSTEM DEVELOPMENT FOR THE STUDY OF GERMANIUM SURFACES WITH  
ATOMIC WIRES**

**M.Sc. THESIS**

**Dilek YILDIZ**

**Department of Physics Engineering**

**Physics Engineering Programme**

**MAY 2014**



**ISTANBUL TECHNICAL UNIVERSITY ★ GRADUATE SCHOOL OF SCIENCE**  
**ENGINEERING AND TECHNOLOGY**

**INVESTIGATION OF GRAPHENE/HOPG SYSTEM AND UHV  
SYSTEM DEVELOPMENT FOR THE STUDY OF GERMANIUM SURFACES WITH  
ATOMIC WIRES**

**M.Sc. THESIS**

**Dilek YILDIZ  
(509121104)**

**Department of Physics Engineering**

**Physics Engineering Programme**

**Thesis Advisor: Assoc. Prof. Dr. Oğuzhan GÜRLÜ**

**MAY 2014**



**İSTANBUL TEKNİK ÜNİVERSİTESİ ★ FEN BİLİMLERİ ENSTİTÜSÜ**

**GRAPHENE/HOPG SİSTEMİNİN İNCELENMESİ VE  
GE YÜZEYLERİNİN ATOMİK TELLER İLE ÇALIŞILMASI İÇİN  
UYV SİSTEM GELİŞTİRİLMESİ**

**YÜKSEK LİSANS TEZİ**

**Dilek YILDIZ  
(509121104)**

**Fizik Mühendisliği Anabilim Dalı**

**Fizik Mühendisliği Programı**

**Tez Danışmanı: Doç. Dr. Oğuzhan GÜRLÜ**

**MAYIS 2014**



**Dilek YILDIZ**, a **M.Sc.** student of **ITU Institute of Graduate School of Science Engineering And Technology** student ID **509121104**, successfully defended the thesis entitled **“INVESTIGATION OF GRAPHENE/HOPG SYSTEM AND UHV SYSTEM DEVELOPMENT FOR THE STUDY OF GERMANIUM SURFACES WITH ATOMIC WIRES”**, which she prepared after fulfilling the requirements specified in the associated legislations, before the jury whose signatures are below.

**Thesis Advisor :**      **Assoc. Prof. Dr. Oğuzhan GÜRLÜ**      .....  
İstanbul Technical University

**Jury Members :**      **Prof. Dr. Ferid SALEHLİ**      .....  
İstanbul Technical University

**Assist. Prof. Dr. Nuri SOLAK**      .....  
İstanbul Technical University

**Date of Submission :**      **05 May 2014**  
**Date of Defense :**      **30 May 2014**





***To my dad,***



## FOREWORD

I would like to state that it was quite an adventure to be a member of NANOBEES research group. Thanks to my father I grew up with Jules Verne and Isaac Asimov books. Fantastic Voyage of Asimov was one of my favorites and I believe this was my fantastic voyage.

I have been working in this group since the beginning and I consider myself a lucky one to witness the construction of a new laboratory. It was an interesting and remarkable experience despite the obstacles. I am grateful to Assoc. Prof. Dr. Oğuzhan GÜRLÜ for giving me this opportunity. My favorite source of motivation was his inspirational talks on scientific problems and phenomena. I am indebted him for his valuable time; he always guided me to the best direction during my study.

I am grateful to my family for their constant support in my academic life. More importantly I am happy that I have their absolute love.

I thank to Rifat and Kıvanç, who are former members of NANOBEES research group; we spent quite some time together during the construction of the laboratory. I would like to thank each member of NANOBEES research group for their friendship. Our discussions with Umut, Cem and Toprak during coffee breaks were fun. I need to thank especially Deniz and Umut for their help and sincere support. I wish all of them happy experiments.

I thank to Prof. Dr. Ferid Salehli and Assist. Prof. Dr. Nuri Solak for evaluating my study.

I would like to thank to Prof. Dr. Oğuz Gülseren and Dr. Şener Şen for their collaboration. We had valuable discussions.

I sincerely thank to Prof. Dr. Kees van der Beek for providing the facility for irradiation experiments.

I would like to thank TUBITAK since my work was supported by different 1001 projects with grant numbers 112T818, 109T687. Also a part of this study was made possible by TUBITAK 2505 project with grant number 113F005 and ITU graduate thesis support program.

May 2014

Dilek YILDIZ  
(Physics Engineer)



## TABLE OF CONTENTS

	<u>Page</u>
<b>FOREWORD .....</b>	<b>ix</b>
<b>TABLE OF CONTENTS .....</b>	<b>xi</b>
<b>ABBREVIATIONS .....</b>	<b>xiii</b>
<b>SUMMARY .....</b>	<b>xix</b>
<b>ÖZET .....</b>	<b>xxi</b>
<b>1. INTRODUCTION .....</b>	<b>1</b>
<b>2. EXPERIMENTAL.....</b>	<b>9</b>
2.1 Methods .....	9
2.1.1 Scanning Tunneling Microscopy.....	10
2.1.2 Ultra High Vacuum (UHV) and STM .....	12
2.2 Experimental Set Ups and Sample Preparation Techniques .....	15
2.2.1 Nanosurf EasyScan STM 2 .....	15
2.2.2 Ultra High Vacuum Scanning Tunneling Microscope (UHV-STM) .....	16
2.2.3 Ion Irradiation Facility (France).....	21
2.3 Samples and Sample Preperation .....	21
2.3.1 Dropcast Method for Preperation of Moiré Structures on HOPG .....	21
2.3.2 Cleaving Highly Oriented Pyrolytic Graphite (HOPG) .....	22
2.3.3 Cleaving and UHV Preperation of Ge(001).....	22
2.3.4 Swift Heavy Ion (SHI) Irradiation .....	24
<b>3. HOPG – MOIRÉ SYSTEM .....</b>	<b>25</b>
<b>4. IRRADIATED HOPG AND MOIRE .....</b>	<b>33</b>
<b>5. GERMANIUM(001) SURFACE.....</b>	<b>41</b>
<b>6. CONCLUSION AND FUTURE WORK.....</b>	<b>43</b>
<b>REFERENCES .....</b>	<b>47</b>
<b>CURRICULUM VITAE .....</b>	<b>59</b>



## ABBREVIATIONS

<b>STM</b>	: Scanning Tunneling Microscopy
<b>nm</b>	: nanometer
<b>SHI</b>	: Swift Heavy Ion
<b>HOPG</b>	: Highly Oriented Pyrolytic Graphite
<b>UHV</b>	: Ultra High Vacuum
<b>Ge</b>	: Germanium
<b>AFM</b>	: Atomic force microscopy
<b>Au</b>	: Gold
<b>nA</b>	: nano Ampere
<b>mV</b>	: mili volt
<b>ITU</b>	: Istanbul Technical University
<b>Ir</b>	: iridium
<b>GMP</b>	: Geometric moire periodicity
<b>RMP</b>	: Real moire periodicity
<b>U</b>	: Uranium
<b>Xe</b>	: Xenon
<b>Pt</b>	: Platinum
<b>XPS</b>	: X-ray photo electron spectroscopy
<b>LEIS</b>	: low energy ion scattering
<b>LEED</b>	: low enegy electron diffraction
<b>RHEED</b>	: reflected high energy electron diffraction
<b>SEM</b>	: Scanning electron microscopy
<b>Si</b>	: Silicon
<b>I</b>	: current
<b>V</b>	: bias
<b>LDOS</b>	: Local density of states
<b>mbar</b>	: milibar
<b>k</b>	: Boltzman constant
<b>OFC</b>	: oxygen free copper
<b>TSP</b>	: titanium sublimation pump
<b>Ti</b>	: titanium
<b>IG</b>	: ion gather
<b>N<sub>2</sub></b>	: nitrogen
<b>K</b>	: Kelvin
<b>STS</b>	: Scanning tunneling spectroscopy
<b>DOS</b>	: Density of states
<b>App</b>	: Appendix





## LIST OF FIGURES

	<u>Page</u>
<b>Figure 1.1</b> : HOPG model and typical STM image of HOPG with atomic resolution. Tunneling parameters, $I = 0.5$ nA, $V_b = 50$ mV. ....	1
<b>Figure 1.2</b> : Ankara goat [5]. Mukhayyar was used for the silk of Ankara Goat.....	2
<b>Figure 1.3</b> : Moire pattern on ITU entrance due to the honeycomb structure.....	2
<b>Figure 1.4</b> : Moiré pattern models on hexagonal lattices with different rotation angles. ....	3
<b>Figure 1.5</b> : STM images of atomic resolution (left) and moire pattern on HOPG. $I = 0.5$ nA, $V_b = 50$ mV for atomic resolution and $I = 0.7$ nA, $V_b = -430$ mV for moire structure. Moiré period was 12 nm.....	4
<b>Figure 1.6</b> : STM images of atomic resolution on HOPG (left) and moiré pattern between the moire boundary and step (right). Tunneling parameters, $I = 0.5$ nA, $V_b = 50$ mV for atomic resolution and $I = 0.7$ nA, $V_b = -300$ mV for moiré structure. Moire period: 7 nm.....	4
<b>Figure 1.7</b> : Generated moiré pattern and zoom in on the moiré spots (GMP= 1.6 nm). The spots are lookalike from far but they are different at atomic level. Red dots represent carbon atoms; green spots represent calculated density of states (DOS) for this system.....	5
<b>Figure 1.8</b> : STM images of 130 MeV $^{238}\text{U}^{31+}$ irradiated HOPG with hillock like structures. Tunneling parameters, $I = 0.5$ nA, $V_b = -50$ mV for both image. ....	6
<b>Figure 1.9</b> : Atomically resolved STM image of hillock like structure. Tunneling parameters $I = 0.5$ nA, $V_b = -50$ mV for both image. ....	7
<b>Figure 1.10</b> : STM image of Ge dimers (left) and a model for $2 \times 1$ reconstruction on Ge (001) surface (right). ....	8
<b>Figure 1.11</b> : Metal/semiconductor interfaces and surfaces: (left) STM image (200 nm $\times$ 20 nm) of about 1 ML Pt film annealed on Ge(001) surface. (right) 3 nm $\times$ 3 nm STM image of Pt nanowires on Ge(001) surface, individual Pt atoms can be picked up with an STM tip. ....	8
<b>Figure 2.1</b> : Representative image of quantum tunneling from sample to tip. $\Phi$ is the work function of the sample. Region 2 represents the potential barrier (and in case of the STM it is the gap between the tip and the sample). ....	10
<b>Figure 2.2</b> : STM setup with its electronic and scan head (left) and zoom in on scan head to show sample and tip (right).....	11
<b>Figure 2.3</b> : STM image of the Ge dimers in filled and empty state to show DOS measurement by STM (left) and its model (right). ....	11
<b>Figure 2.4</b> : Photo of UHV system on its frame in our laboratory which was constructed during this study. ....	13
<b>Figure 2.5</b> : Nanosurf Easyscan STM head with sample and tip. ....	15
<b>Figure 2.6</b> : Optical image of mechanically cut $\text{Pt}_{80}\text{Ir}_{20}$ tip.....	16
<b>Figure 2.7</b> : Additional homemade parts of UHV system. Sample fork (upper images), Pt evaporator (middle) and sample carrier (bottom). ....	17

<b>Figure 2.8 :</b> Making the vibration isolation table. Preperation of the isolation system (upper images), drawing of the table (bottom-left) and the table itself (bottom-right) .....	18
<b>Figure 2.9 :</b> Pumps of UHV system. Rough pump, turbo pump, ion pump (in order from left to right).....	18
<b>Figure 2.10 :</b> UHV STM head (left) and linear and rotational feedthroughs (right)..	19
<b>Figure 2.11 :</b> UHV STM head (left) and zoom in on tip-sample (right).....	20
<b>Figure 2.12 :</b> On the left image, NANONIS STM control unit and UHV system behind it. Femto I/V converter is on the right image. ....	20
<b>Figure 2.13 :</b> STM image of rough Au surface with UHV-STM and NANONIS control electronic. Image size 64 nm × 64 nm, I= 0.2 nA, V = 100 mV. Measurement was done under ambient conditions. ....	21
<b>Figure 2.14 :</b> Cleaved HOPG crystal. Topmost layers of HOPG crystal was peeled of by scotch tape. Sevreal stick-and-pull procedures were applied as seen on the tape (to the left). ....	22
<b>Figure 2.15 :</b> Ge cleaving by diamond pen (upper left image), cleaved Ge crystal (upper right image) and mounted on sample holder on the fork (bottom images).....	23
<b>Figure 2.16 :</b> Designed parts (left) and assembly (middle) of sample holder on the left side. Two assembled sample holders. ....	23
<b>Figure 3.1 :</b> Raman spectrum of cyclohexane dropcasted HOPG surface and cyclohexane solution. The moiré sample only shows the peaks intrinsic to the HOPG surface.....	25
<b>Figure 3.2 :</b> List of used chemicals in preparation of moiré structures on HOPG. Observed periodicities were added to compare the effect of each chemical. ....	26
<b>Figure 3.3 :</b> Atomic resolution on HOPG (left) and on moiré structure (right). Tunneling parameters I= 0.5 nA, V <sub>b</sub> = - 50 mV. GMP = 1.6 nm. ....	27
<b>Figure 3.4 :</b> STM image of moiré structure in large area on the left (I= 0.5 nA, V= - 200 mV). Zoom in STM image on the boundary of the moiré structure with atomic resolution at high bias (right) (I= 0.5 nA, V <sub>b</sub> = -500 mV)....	28
<b>Figure 3.5 :</b> Corrugation analyses of moiré structure. (STM image of moiré pattern with atomic resolution and line scans on each direction of the pattern on the left (I= 0.5 nA, V <sub>b</sub> = -45 mV, GMP = 2.54 nm).....	28
<b>Figure 3.6 :</b> (a) Curves of corrugation change with respect to bias (three different moiré patterns). (b) STM image of moiré pattern. Bias was changed from -50 mV to -800 mV during scanning. (c) - (g) STM images of the same moiré pattern with different bias. (h) Charge plot of calculated DOS of moiré unit cell (GMP=1.6 nm, RMP = 2.84) (Theoretical calculations were done on moire systems, please see the Appendix B). ....	29
<b>Figure 3.7 :</b> STM images of moiré pattern with atomic resolution. Left image was typical STM image of moiré pattern with atomic resolution. STM image on the right shows contrast reversal on moiré structure, triangular structure switched to hexagonal during STM study. And bright moire spots became dark. Scanning parameters were I=0.4 nA, V <sub>b</sub> = -50 mV, GMP = 1.6 nm.....	30
<b>Figure 3.8 :</b> STM image of contrast reversal on moiré pattern on graphene/Ir(111) system. (I= 15nA and V <sub>b</sub> changed from -0.5 V to -1.8 V) [39]. ....	31
<b>Figure 3.9 :</b> LDOS curves of HOPG and moiré patterns on HOPG (GMP of the patterns were 1.6 nm and 1.8 nm)) system. Arrows points the	

shoulders due to the van Hove singularity. (See Appendix B for theoretical calculations).	32
<b>Figure 4.1 :</b> STM image of SHI irradiated Goodfellow-HOPG surface in large scale (left) ( $I = 0.4$ nA, $V = -75$ mV). STM image on the left shows HOPG surface with irradiation defects ( $I = 0.3$ nA, $V = -100$ mV).	34
<b>Figure 4.2 :</b> STM image of defects due to the irradiation on Goodfellow-HOPG surface (left) ( $I = 0.4$ nA, $V = -75$ mV). STM image of the defects with atomic resolution ( $I = 0.3$ nA, $V = -100$ mV).	34
<b>Figure 4.3 :</b> STM image of defects due to the irradiation, a different area (Goodfellow-HOPG surface) on the left ( $I = 0.3$ nA, $V = -100$ mV). STM image of marked defect with atomic resolution ( $I = 0.4$ nA, $V = -50$ mV).	35
<b>Figure 4.4 :</b> Large area STM image of irradiated SPI-HOPG with moiré pattern due to dropcasted cyclohexane ( $I = 0.3$ nA, $V = -50$ mV). Black circles show the irradiation defects.	36
<b>Figure 4.5 :</b> STM image showing the apparent clustering direction of the defects on moiré and clean part of HOPG surface. Red line shows the direction of the defect on moiré patterned area and black lines show the direction of the defect on clean part of HOPG ( $I = 0.3$ nA, $V = -50$ mV). The direction of the black lines were the same and angle between the directions of the red and the black lines was $8^\circ$ .	36
<b>Figure 4.6 :</b> Zoom in STM image of SHI irradiation defect on HOPG (circle shows the defect on the left image) ( $I = 0.4$ nA, $V = -50$ mV).	37
<b>Figure 4.7 :</b> Zoom in STM image of SHI irradiation defect on moiré on HOPG (circle shows the defect on the left image) ( $I = 0.4$ nA, $V = -50$ mV).	38
<b>Figure 4.8 :</b> STM images of irradiation defects on HOPG and on moiré ( $I = 0.4$ nA, $V = -50$ mV).	38
<b>Figure 4.9 :</b> STM image of two different SHI irradiation defects on SPI-HOPG ( $I = 0.3$ nA, $V = -50$ mV).	39
<b>Figure 4.10 :</b> STM images of single ( $I = 0.3$ nA, $V = -50$ mV) and cluster ( $I = 0.3$ nA, $V = -50$ mV) irradiation defects on Goodfellow and SPI HOPG.	40
<b>Figure 5.1 :</b> STM image of Ge(001) surface with dimers. ( $I = 300$ pA, $V_b = -1.55$ V) the dimer rows on every second terrace can be seen in the left image with a $45^\circ$ degree orientation with respect to the image axes.	41
<b>Figure A. 1</b> Approach mechanism of UHV-STM. By using the rotational feedthrough (a) worm gear (b) is rotated. Sample is approached by rotated worm gear. (d) & (e) sample approached.	52
<b>Figure B. 1:</b> Generation of moiré pattern (left). Generated moiré pattern, inset image shows calculated charges for this pattern.	53
<b>Figure B. 2:</b> Calculated band structure of (a) m1n10 moire structure, (b) m1m12 moire structure with ab initio. Calculated band structure of (c) m1n11 moire structure (d) m1n7 moire structure between high symmetry points M and M'. (e) Band dispersion around high symmetry point K for various systems which exhibits linear and second order behaviour.	53
<b>Figure C.1:</b> Height profiles of irradiation defects on GF-HOPG. (a) triple defects (b) single defect.	54
<b>Figure C.2:</b> Height profiles of irradiation defects on SPI-HOPG. The defects on HOPG part were like triple defect on a line. It was not multiple separated point defects but spreaded defect on a line. Unlike the multiple defects on Goodfellow HOPG, the multiple defects on SPI HOPG were ordered. The height of the multiple defects on SPI HOPG	

	was lower and width of them was wider. Still atomic resolution on or around the defect was not observed. ....	55
<b>Figure C.3:</b>	Height profiles of irradiation defects on moire structures on SPI-HOPG. Unlikely the defect on HOPG part, the defect on moiré pattern was like a line defect. It was not multiple separated point defects but spreaded defect on a line. Clearly, the defect on moiré pattern was more narrow and longer. Atomic resolution on or around the defect was not observed. Still defect formations were different on moiré pattern and HOPG. ....	56
<b>Figure C.4:</b>	Height profile of single defects on SPI-HOPG. Atomic resolution on the defect was observed on single irradiation defect on SPI-HOPG (left). The apparentheight of this defect was measured as 77 pm. Apparent height of the defect on the right was 130 pm and it was not possible to achieve atomic resoluoyion on the defect. It is possible that achieving atomic resolution on or around the defect depends on the height of the defect. ....	57
<b>Figure C.5:</b>	Bias dependent height profile on single defect on SPI HOPG. Heights of the defects decrease with increasing tip bias. Altough atomic reconstruction were not observed on irradiated HOPG surfaces, changing of the apparent heights of the defects show that irradiation defects change the electronic properties of HOPG.....	58

## **INVESTIGATION OF GRAPHENE/HOPG SYSTEM AND UHV SYSTEM DEVELOPMENT FOR THE STUDY OF GE SURFACES WITH ATOMIC WIRES**

### **SUMMARY**

We probably know quite a lot on the bulk properties of materials but we barely know the surface properties of them. With the help of scanning tunneling microscopy (STM), surface structures can be investigated with 0.1nm lateral resolution. This thesis includes the investigation of super periodic structures (moiré patterns) and swift heavy ion (SHI) irradiation defects on HOPG and construction of an Ultra High Vacuum (UHV) system for the study of atomic wires on Ge(001) surface.

Highly oriented pyrolytic graphite (HOPG) is a common crystal for STM studies because of its inert and smooth surface. Even atomic resolution on HOPG can be achieved under ambient conditions by using STM. HOPG has layered structure and there is van der Waals bond between its layers. Crystal can be cleaved with sticky tape due to the weak van der Waals interaction. Fresh and clean surface can be obtained by cleaving this layered crystal. As another result of the weak van der Waals bonding, the topmost layer of HOPG crystal may be rotated by chemical or mechanical means. Due to the rotation of the topmost layer, superperiodic structures called as moiré patterns occur. These structures were known for years but they were rediscovered in graphene research. Although these structures were studied for a long time by many different research groups, their origin are yet to be understood. These structures can be studied with STM but they are invisible to atomic force microscopy (AFM) so far. In this study, preparation method of moiré structures on HOPG were improved. Morphological and electronic structures of the moiré patterns on HOPG surfaces were studied with STM. Poor man's spectroscopy and scanning tunneling spectroscopy (STS) were performed on these structures.

Besides the super periodic structures, Swift Heavy Ion (SHI) Irradiation defects on HOPG surfaces were investigated in this study. Defect formation on layered structures is popular because hillock like structures and atomic reconstruction can be observed on irradiated surfaces. Although HOPG is a well known crystal, properties of HOPG change with the supplier. Therefore SHI defects on HOPG crystals were observed and the defect formation was compared with respect to the supplier. As moiré patterns have different structure (both electronic and morphological) than HOPG, we also studied defect formation due to the SHI on moiré patterned surfaces.

Other than the STM study on graphitic surfaces, a UHV system was constructed to investigate atomic wires on Germanium (Ge) surfaces. A vibration isolation system was designed and constructed for the UHV system. UHV-STM was tested with polycrystalline gold (Au) samples under ambient conditions. Ge (001) surface was prepared under UHV conditions and Ge terraces were observed with UHV-STM. Moreover dimer rows due to (2x1) reconstruction of the Ge(001) surface was observed.



## GRAPHENE/HOPG SİSTEMİNİN İNCELENMESİ VE GE YÜZEYLERİNİN ATOMİK TELLER İLE ÇALIŞILMASI İÇİN UYV SİSTEM GELİŞTİRİLMESİ

### ÖZET

Kristallerin kütsel (bulk) özellikleri oldukça iyi bilinmesine rağmen yüzey özellikleri pek de bilinmemektedir. Taramalı tünelleme mikroskopisi (TTM) sayesinde 0.1 nm çözünürlükle yüzey özellikleri çalışılabilir. Bu çalışma çok düzenli pirolitik grafit (HOPG) üzerinde görülen moiré desenleri olarak adlandırılan süper periyodik yapılar ve hızlı ağır iyonlarla (swift heavy ion (SHI)) bombardıman edilmiş HOPG yüzeylerinin TTM ile incelenmesini içermektedir. Bunun yanında Ge (111) yüzeyinde oluşturulan atomik tellerin çalışılabilmesi için bir ultra yüksek vakum (UYV) kazanının kurulması ve geliştirilmesi de bu tez çalışmasına gerçekleştirilmiştir.

HOPG, soy ve düzgün bir yüzey olduğu için TTM çalışmalarında sıkça kullanılan bir kristaldır. Hatta TTM ile bu kristal yüzeyinde, atmosferik koşullarda atomik çözünürlük elde etmek mümkündür. HOPG katmanlı bir yapıya sahiptir ve katmanlar arasında zayıf van der Waals etkileşimi vardır. Bu zayıf etkileşimin bir sonucu olarak üstte bulunan katmanlar bant yardımı ile kaldırılabilir (cleaving). Kristalin üst katmanlarının kaldırılması ile birlikte temiz kristal yüzeyi elde edilir ve bu sayede aynı kristal tekrar tekrar kullanılabilir. Kristalin bu kadar basit bir şekilde temizlenebilir olması çok büyük bir avantajdır. Kristal katmanlı bir yapıya sahip olduğu için bant yapıştırma sırasında baskı uygulanması ya da bant ile katmanlar kaldırılırken hızlı davranılması kristale zarar verebilir. Bu sebeple temizleme işlemi sırasında kristala çok fazla baskı uygulanmamalıdır. Katmanlar arasındaki zayıf etkileşimin diğer bir sonucu olarak HOPG'nin en üst katmanı kimyasal ya da mekanik yollarla kristal yüzeyinde döndürülebilir. Katmanın dönme açısına bağlı olarak süper periyodik yapılar oluşur. Bu süper periyodik yapılara moiré desenleri desenleri. İki periyodik yapının üst üste gelmesi ve optik ilizyon sonucu gözlenen bu moiré desenleri günlük hayatımızda pek çok yerde karşımıza çıkmaktadır. Bu yapılar çitlerde, tüllerde ve hatta kuş tüylerinde görülmektedir. Sıkça rastladığımız ve optik olarak gözlenen bu yapıların atomik ölçekte de görülmesi oldukça enteresandır. HOPG'nin en üst katmanının döndürülmesi ile oluşan moiré desenleri uzun yıllardır bilinmesine rağmen, grafen çalışmaları ile birlikte yeniden ilgi odağı olmuşlardır. Ayrıca bu desenlerin elektronik mi yoksa yapısal mı olduğu sorusuna net bir cevap çıkmamıştır. Moiré desenleri TTM ile araştırılmaktadır ancak şimdiye kadar atomik kuvvet mikroskobu ile gözlenen moiré deseni rapor edilmemiştir.

Bu çalışmada moiré desenlerinin HOPG üzerinde elde edilmesi için hazırlama yöntemi geliştirilmiştir. Daha önceki çalışmalarda belirtildiği üzere HOPG kristalini kimyasala daldırıp bekleterek moiré deseni elde etmek mümkündür ancak HOPG katmanlı bir yapıya sahiptir ve kimyasal HOPG katmanları arasına girerek tüm kristale zarar vermektedir. Yaptığımız bu çalışmada moiré desenlerini elde etmek için kloroform, sikloheksan, toluen gibi uçucu kimyasallar HOPG yüzeyine damlatılmış ve kimyasalın moiré deseni oluşumuna etkisi olup olmadığı araştırılmıştır. Her örnek kimyasal damlatılmadan önce scotch tape ile cleave

edilerek temizlenmiştir. Kimyasalları damlatmak için otomatik mikropipet ve tek kullanımlık pipet ucu kullanılmıştır. Pipet ucundan kaynaklanacak olası kirlilikleri önlemek için pipet uçları kimyasal damlatmadan hemen önce damlatılacak kimyasal ile temizlenmiştir. Yapılan çalışmada bazı kimyasalların moiré oluşumuna etkisi çok olmasada moiré desenine rastlanmış ancak siklohekzan damlatılan her yüzeyde moiré deseni gözleendiği belirlenmiştir. Siklohekzan damlatılarak hazırlanan örneklerde görüldüğü üzere bu yöntem tekrar edilebilir ve oldukça kolay bir yöntemdir. HOPG kristaline kimyasal damlatmak kritale zarar vermemektedir ve standart HOPG temizleme prosedürü (scotch tape ile cleave ederek) uygulanarak kimyasal damlatılmış yüzeyden de kurtulmak mümkündür.

Çalışmanın devamında HOPG üzerinde elde edilen moiré desenlerinin yapısal ve elektronik özellikleri TTM ile çalışılmıştır. Hazırlanan örneklerde periyodu 1.6nm'den 30nm'ye kadar değişen farklı moiré desenleri gözlenmiştir. Yapılan çalışmada moiré desenleri üzerinde atomik çözünürlük de gözlenebileceği gösterilmiş ve HOPG ve moiré üzerinde gözlenen atomik çözünürlüğün farkları ortaya konmuştur. HOPG üzerinde atomik çözünürlük 50mV civarında gözlenebilir ancak yüksek gerilim voltajlarında bu mümkün değildir. Moiré desenlerinde ise 50mV gübü düşük gerilim voltajında atomik çözünürlük gözlediği gibi 500mV gibi yüksek gerilim voltajına kadar çözünürlük elde etmek mümkündür. Moiré desenlerinin gözlenen yükseklikleri tünelleme eklemi gerilim voltajına bağlı olarak incelenmiştir. Bu çalışmada üç farklı moiré örneği kullanılmıştır ve periyodları farklıdır. Moiré desenlerinin gözlenen yükseklikleri tünelleme eklemi gerilimi arttıkça azaldığı görülmüştür. Moiré desenlerinin hepsinde gözlenen yükseklikler artan gerilim voltajına bağlı olarak azalmaktadır; bu azalma üç örnekten ikisinde lineerdir ve bir tanesinde azalma ile birlikte dalgalanma da gözlenmiştir. Bu dalgalanma moiré yapılarında farklı elektronik durumlar olabileceğini göstermektedir. Bu yapılar üzerinde TTM çalışmalarının yanında tünelleme spektroskopisi (TTS) de yapılmıştır. Tünelleme eklem gerilimine bağlı akım ölçülmüş ve buradan tünelleme eklem gerilimine bağlı yerel elektron durum yoğunluğu grafiği elde edilmiştir. Bu grafikler göstermektedir ki moiré desenlerinin elektronik yapısı HOPG'den oldukça farklıdır. Hatta grafen ile benzerlik göstermesine rağmen moiré desenleri ile grafenin farklı yapılar olduğu rahatlıkla söylenebilir. Bu durumda moiré desenleri HOPG üzerinde bulunan büyük bir molekül gibi değerlendirilebilir.

Süper periyodik yapılar yanında yüksek enerjili ağır iyonlar (Swift Heavy Ion (SHI)) ile bombardıman edilen HOPG yüzeylerindeki kusurlar da TTM ile incelenmiştir. Kristal SHI ile yüksek enerjilerde bombardıman edildiğinde iyon kristaldeki elektronlar ile etkileşir ve iyon geçtiği yolda iz bırakır. Ayrıca bombardıman sonrasında yüzeyde de kusurlar gözlenmektedir. Bu kusurlar iyon enerjisi ve tipine bağlı olabileceği gibi kristalin külçe yapısı ve külçedeki kusurlara da bağlıdır. SHI ile bombardıman edilen katmanlı yapılar, kusurların katmanlı yapılarda oluşması ve tepelik benzeri yapılar ile bu yapıların civarında atomik ölçekte yeniden yapılanma gözleendiği için ön plandadır. HOPG iyi bilinen bir kristal olmasına rağmen, kristalin özellikleri temin edilen firmaya göre değişmektedir. Bu sebeple farklı firmalardan temin edilen HOPG kristalleri SHI ile bombardıman edilmiş ve kusur oluşumu karşılaştırılmıştır. Moiré yapıları HOPG'den farklı yapısal ve elektronik özelliklere sahip olduğu için moiré örnekleri hazırlanmış ve bu örnekler de SHI ile bombardıman edilmiş ve moiré desenleri üzerinde kusur oluşumu incelenmiştir. Yapılan çalışmada TTM kullanılarak HOPG üzerinde tek ve çoklu kusurlar gözlenmiş ve aynı kristal yüzeyinde dahi kristalin külçe özelliklerine bağlı olarak kusur tipinin değiştiği görülmüştür. Yüzeydeki kusurların incelenmesiyle kristalin



külçe özellikleri ile ilgili bilgi edinilebileceği anlaşılmıştır. Bombardıman edilen moiré örnekleri TTM ile incelenmiş ve moiré yapısının iyon bombardımanına karşın bozulmadığı gözlenmiştir. Beklendiği gibi, aynı kristal yüzeyinde olmasına rağmen kristal oluşumunun HOPG ve moiré yüzeyi üzerinde farklı olduğu TTM ölçümleri ile gösterilmiştir.

Bu tez çalışması kapsamında bir Ultra Yüksek Vakum (UYV) Sistemi Ge (001) yüzeyi üzerinde oluşan atomik tellerin hazırlanması ve bu yapıların yapısal ve elektronik özelliklerinin çalışılması için kurulmuştur. Sistem için titreşim izolasyon masası tasarlanmış ve yapılmıştır. İzolasyon masası için optik masalarda kullanılan izolasyon bacaları satın alınarak temin edilmiştir. Bacaklar üzerine yerleştirilen iskelet için 6m uzunluğunda alüminyum profiller temin edilmiş ve radyal testere yardımıyla kesilerek gerekli uzunluklarda parçalara ayrılmıştır. Bu parçaların birleştirilmesi ile de iskelet yapılmıştır. UHV kazanı kurulduktan sonra ultra yüksek vakum elde etmek için gerekli olan iyon pompası bağlantıları yapılmıştır. İyonpompası ve pompanın güç kaynağı farklı şirketlerden olduklarından yeni bir bağlantı yapılması gerekmiştir. Daha sonra örneği kazan içinde hareket ettirmek ve manipule edebilmek için gerekli çatalın bağlantıları yapılmıştır. Sistemin çalışması için gerekli eklemeler yapıldıktan sonra platin buharlaştırıcısı da laboratuarda yapılmıştır. Buharlaştırıcı için bakır bloklar ve tungsten teller kullanılmıştır. Tungsten teller rezistans olarak kullanılmış ve bakır bloklar tungsten telleri desteklemek için kullanılmıştır. Tüm eklemelerden sonra sistem vakuma alınmış ve  $5 \times 10^{-10}$  mbar'dan daha düşük bir basınca gidilebilmiştir.

UYV-TTM sistemi havada altın (Au) yüzeyi ile test edilmiştir. Bu test sırasında tüm mekanik ve elektronik gürültü kaynakları bulunup, ortadan kaldırılmıştır. Örnek tutucular ve TTM kafasında gerekli yerler kontrol edilmiş, eksikler giderilmiştir. Sistemdeki tüm elektriksel bağlantılar kontrol edilmiş ve testleri yapılmıştır. Au üzerinde beklediği gibi bir TTM datası elde ettikten sonra UYV-TTM UYV kazanına takılmış ve vakumdaki testleri yapılmıştır. Sistem vakuma alındıktan sonra Ge(001) hazırlama işlemine geçilmiş, Ge(001) yüzeyi UYV altında hazırlanmış ve kristal terasları UYV-TTM ile gözlenmiştir. Ge(001) yüzeyinin temizlenmesi ve hazırlanması için örnek ısıtılmış, argon sıçratma uygulanmış ve tekrar ısıtılmıştır. Temizlenen Ge(001) yüzeyinde, Ge terasları, dimer çubukları ve Ge-dimerleri (Ge ikili molekülleri) gözlemlenebilmiştir. Ge(001) yüzeyinde dimerlerin gözlenmesi hem UYV sisteminin (tüm eklenen parçaları ile birlikte), hem de UYV-TTM'nin çalıştığını göstermektedir.



## 1. INTRODUCTION

Highly Oriented Pyrolytic Graphite (HOPG) can be considered as the drosophila of surface science, especially for the scanning probes. HOPG is a quite popular crystal in surface science because of its smooth and chemically inert surface. It is commonly employed as a calibration sample for scanning tunnelling microscopy (STM) studies. HOPG is composed of Bernal stacked two dimensional hexagonal lattices with carbon atoms at the lattice sites, popularly named as graphene layers [1,2]. Atoms in topmost layer are named as  $\alpha$  or  $\beta$  atoms; while there is an atom under  $\alpha$  atoms,  $\beta$  atoms sit at the center of a hexagons of the lower layer. Due to the interaction between  $\alpha$  atoms and the atoms below them,  $\alpha$  atoms have lower density of states than  $\beta$  [2]. As  $\beta$  atoms have higher density of states, triangular structure is observed on most atomic resolution STM image of HOPG at low bias. Figure 1.1 shows the model of HOPG (with  $\alpha$  and  $\beta$  atoms) and atomically resolved STM image on HOPG. Depending on the bias voltage and tip-sample combination, it is possible to observe all atoms.

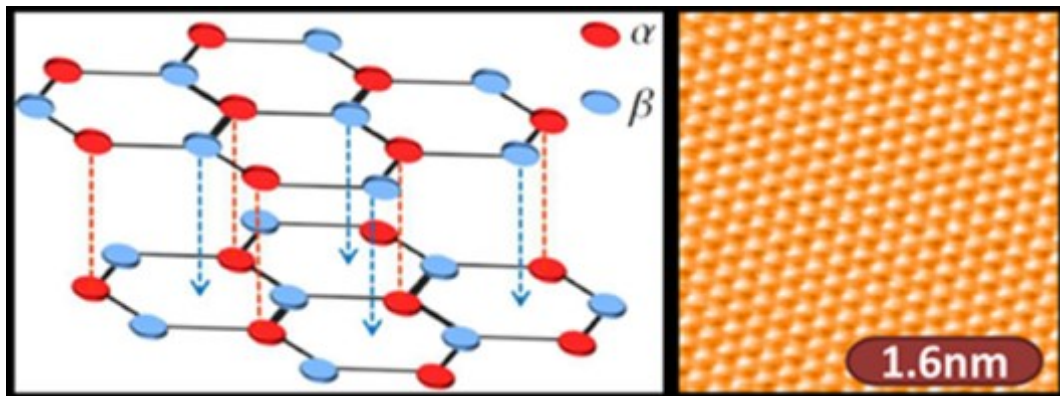


**Figure 1.1** : HOPG model and typical STM image of HOPG with atomic resolution. Tunneling parameters,  $I = 0.5$  nA,  $V_b = 50$  mV.

Nearest neighbour carbon atoms in a layer are bonded strongly with each other. Unlike the atoms of a single layer, the layers are not strongly bonded (only by van der Waals bonds); so that the layers can be cleaved with sticky tape and this way fresh and clean surfaces can be obtained [2-4].

Moire, as a word, has an interesting origin as it was derived from an Arabic word mukhayyar [5]. Mukhayyar was used for the silk of Ankara Goat to describe its

perfect texture. Its silk has wavy appearance when it gets wet. Later, the word was used for textiles.



**Figure 1.2 :** Ankara goat [5]. Mukhayyar was used for the silk of Ankara Goat.

On the other hand, moire patterns are super periodic patterns that we are familiar from our daily lives. These patterns are observed on clothes, fences, cages, screens of computes or feathers of birds. Such pattern can be seen on main entrance of Istanbul Technical University (ITU) (figure 1.3).



**Figure 1.3 :** Moire pattern on ITU entrance due to the honeycomb structure.

Basically, an interference pattern of different periodic structures can be called as moiré pattern. It is also possible to observe these patterns on HOPG. Due to the weak van der Waals bonding between the layers of HOPG, topmost layer may be shifted or rotated by mechanical or chemical means. Because of the rotation of the top layer, super-periodic structures called as moiré patterns form on HOPG surfaces [6-12]. Figure 1.4 shows the model of moiré structures on hexagonal lattices.

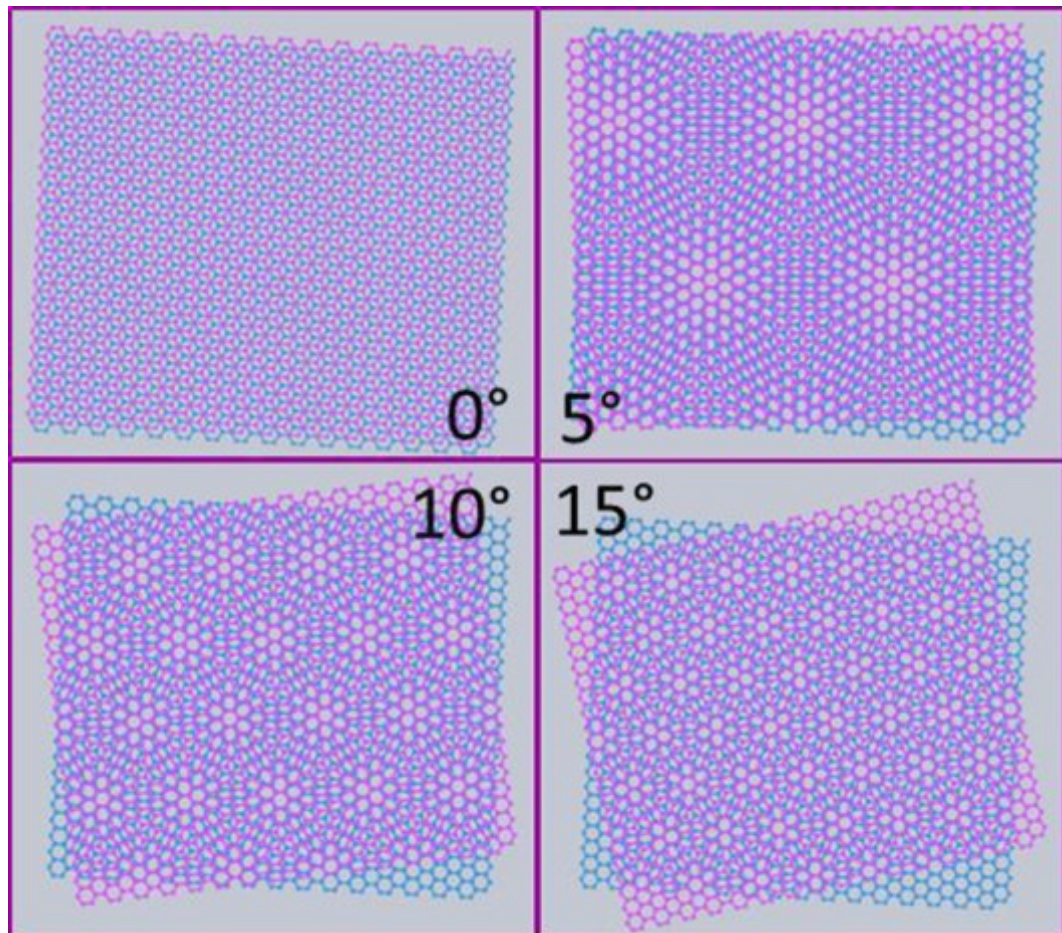


**Figure 1.4 :** Moiré pattern models on hexagonal lattices with different rotation angles.

Moiré patterns occur in nature and they are fascinating phenomena already optically, and when it comes to such structures at the atomic level, understanding their origin becomes even more tedious [12-25]. Since the first observation of moiré patterns on HOPG surfaces, their origin is still a matter of debate [12-37]. Moiré patterns are also observed on graphene on metal systems such as graphene on Ir(111) due to lattice mismatch between graphene and the Ir(111) surface [38, 39]. The origin of moiré pattern on graphene on metal system is structural. Although there is no lattice mismatch between graphene and HOPG, moiré structures are



clearly observed on graphene/HOPG system. Moiré patterns on HOPG are so far invisible to atomic force microscopy (AFM) but they can be investigated with STM.

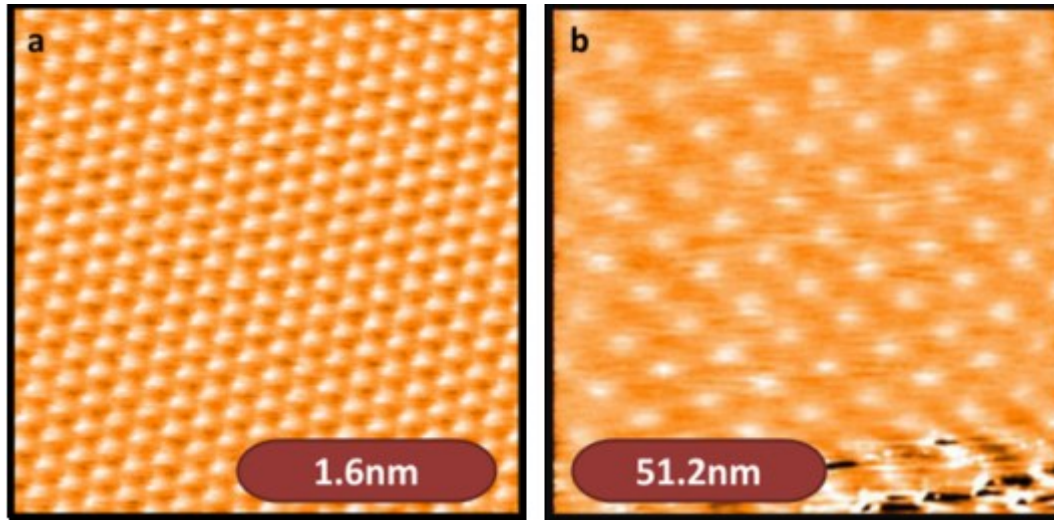


**Figure 1.5 :** STM images of atomic resolution (left) and moiré pattern on HOPG.  $I = 0.5$  nA,  $V_b = 50$  mV for atomic resolution and  $I = 0.7$  nA,  $V_b = -430$  mV for moiré structure. Moiré period was 12 nm.

These structures mostly form near the steps of HOPG and have boundaries called as moiré boundary. Corrugation of moiré boundaries are higher than the rest of the pattern but their periodicities are the same. Surely, periodicities of moiré structures are larger than the lattice parameter HOPG, which is 0.246 nm.

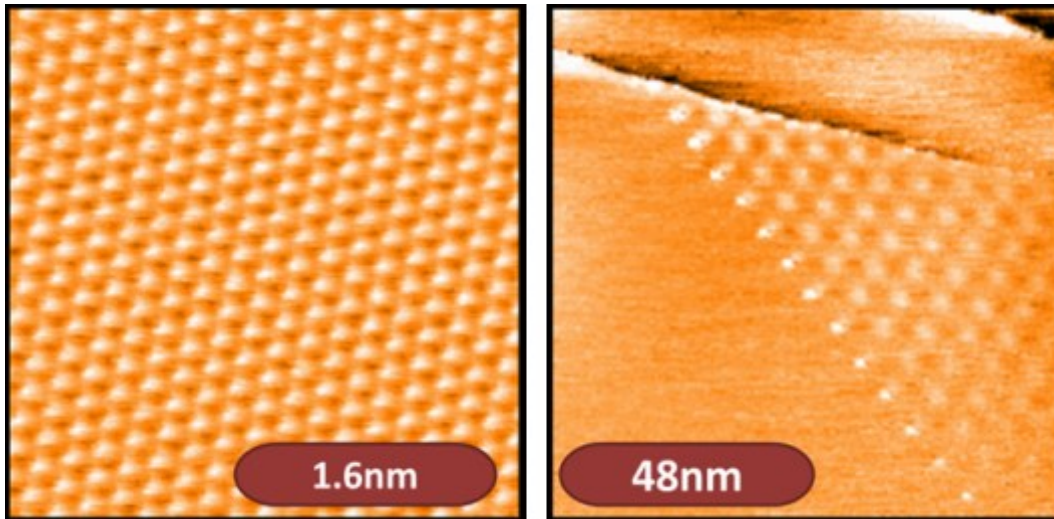


**Figure 1.6 :** STM images of atomic resolution on HOPG (left) and moiré pattern between the moiré boundary and step (right). Tunneling parameters,  $I = 0.5$  nA,  $V_b = 50$  mV for atomic resolution and  $I = 0.7$  nA,  $V_b = -300$  mV for moiré structure. Moiré period: 7 nm.

Concerning the periodicity, moiré periodicity is designated with  $D$ . While  $a_{HOPG}$  is the lattice constant of HOPG and  $\theta_{rot}$  is rotation angle of the topmost layer  $D$  is given with equation below [37].

$$D = \frac{a_{HOPG}}{2 \sin(\frac{\theta_{rot}}{2})} \quad (1.1)$$

This relation indicates the distance ( $D$ ) between the two bright spots, or the round shapes due to super periodic structures. However, brighter spots of moiré structures are not identical at atomic level. Even studying with large structures, one should consider atomic level differences in STM studies. We called  $D$  as the geometric moiré periodicity (GMP). Figure 1.6 shows the unit cell of generated moiré structure with 1.6 nm GMP. Unit cell was generated by rotating the atom positions of two graphene layers. As it can be seen in figure-1.6, the distance between the nearest neighbor round structures, due to the super period, is not the same as the unit cell size of the moiré lattice. Here we called the moiré lattice parameter as the “Real Moiré Periodicity” (RMP) (RMS is simply  $\sqrt{3}D$ ).

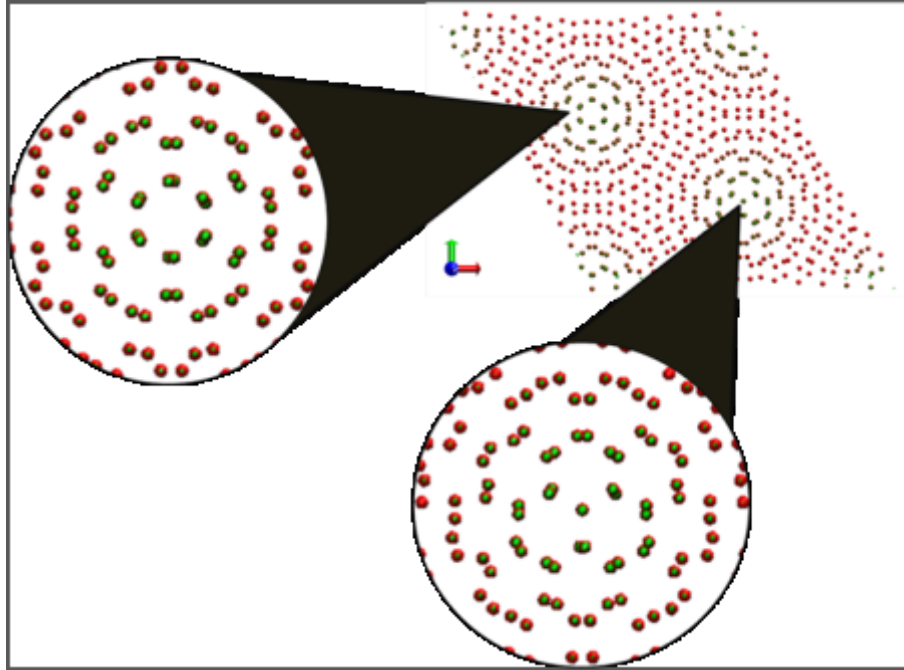


**Figure 1.7 :** Generated moiré pattern and zoom in on the moiré spots (GMP= 1.6 nm). The spots are lookalike from far but they are different at atomic level. Red dots represent carbon atoms; green spots represent calculated density of states (DOS) for this system.

Highly Oriented Pyrolytic Graphite (HOPG) is a well-known crystal as a calibration sample and a substrate for surface studies. It is often overlooked that the electronic and morphological properties of pristine HOPG surfaces can change depending on the supplier. These changes may be negligible at large scales but they are important for SPM studies, especially at the atomic scale when investigated by STM.

Still HOPG is a topic of interest in swift heavy ion (SHI) irradiation studies because of its layered structure. Nuclear stopping is dominated by electron stopping in SHI irradiation and ion tracks are observed in irradiated crystals. Different studies on HOPG surfaces irradiated with swift heavy ions like U and Xe reported hillock like structures [40-42]. We have similar observations like in Figure-1.8.

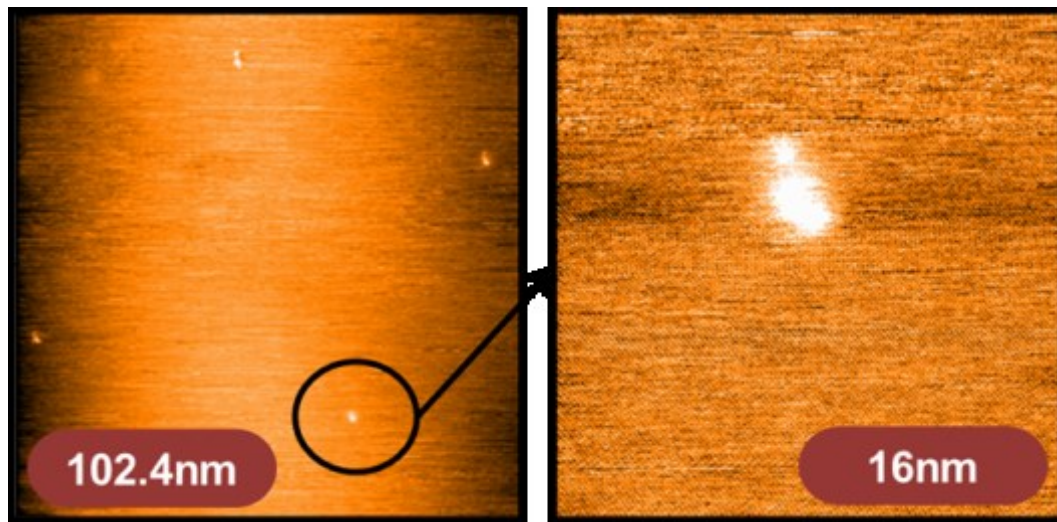


**Figure 1.8 :** STM images of 130 MeV  $^{238}\text{U}^{31+}$  irradiated HOPG with hillock like structures. Tunneling parameters,  $I = 0.5$  nA,  $V_b = -50$  mV for both image.

In fact, those hillock like structures are not hillocks at all, when observed at the atomic level as shown in figure-1.9. Defects were spreaded over the surface and they changed the atomic structure of HOPG surface. Probable local reconstruction at the atomic scale due to swift heavy ion irradiation is yet to be understood. The dependence of the damage on the type of HOPG was not reported earlier, either.



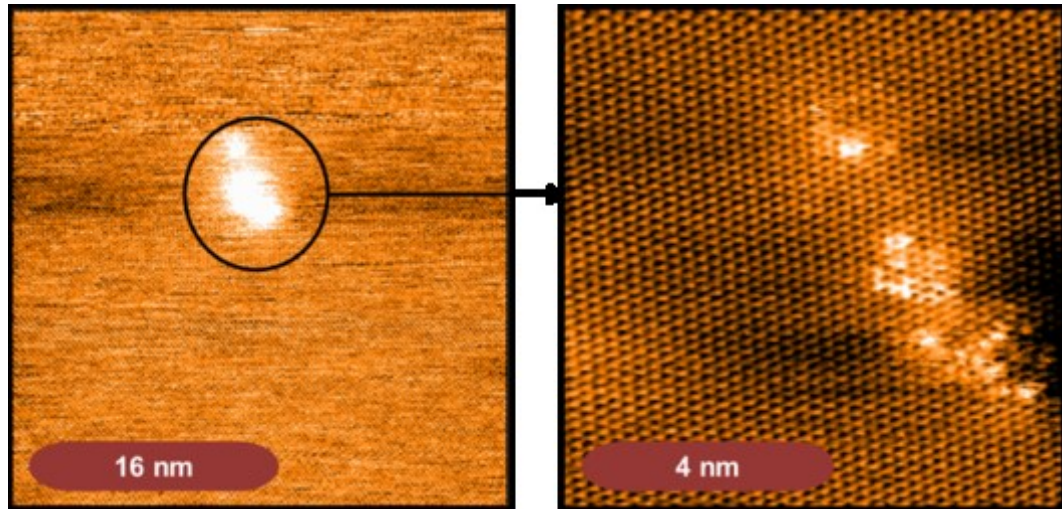


**Figure 1.9 :** Atomically resolved STM image of hillock like structure. Tunneling parameters  $I = 0.5$  nA,  $V_b = -50$  mV for both image.

In addition to the irradiation defects on HOPG surface, the questions on the nature of irradiation related defects on graphene specimens transferred on to dielectric substrates remain [41]. Important point is that the effect of the substrate on defect formation in graphene due to swift heavy ions. Dielectric substrates are damaged by the SHI irradiation as well. Consequently, dielectric substrate damages the graphene rather than the defect formation directly on the graphene. Such damage was not reported in layered structures. Therefore, we were interested in studying SHI irradiated graphene layer with on a native layered structure, namely the HOPG crystal itself.

Germanium (Ge) crystal has diamond lattice structure. On Ge(001) surface, dimer rows can be observed due to the reconstruction, by using UHV-STM. To observe such reconstruction, Ge (001) surface must be treated under UHV conditions [3,42]. STM image of Ge (001) surface and a model of  $2 \times 1$  reconstruction of Ge (001) surface are shown in figure-1.10. Light blue dots represent the atoms on the surface and yellow ellipses represent dimer bonds due to the reconstruction.

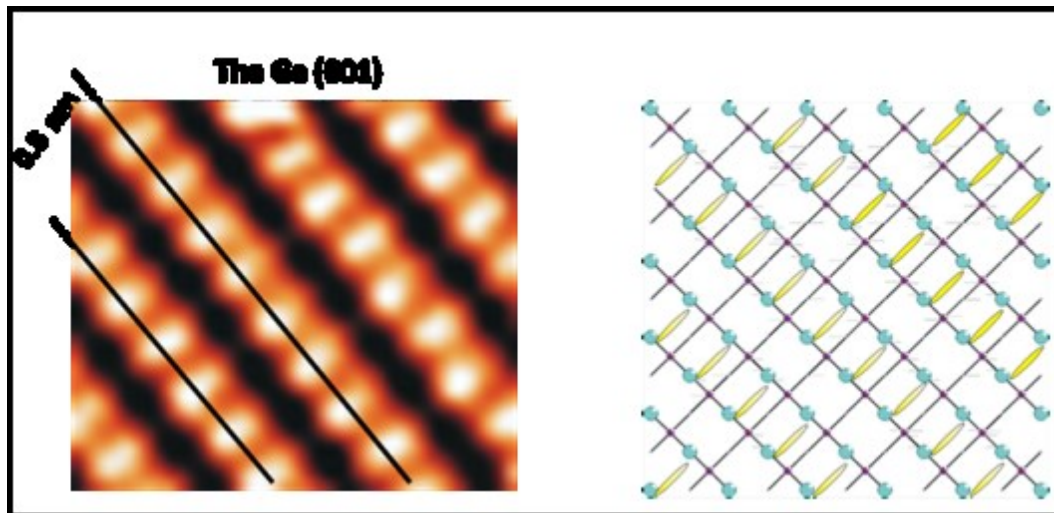


**Figure 1.10** : STM image of Ge dimers (left) and a model for  $2 \times 1$  reconstruction on Ge (001) surface (right).

Ge(001) allows us to prepare metal/semiconductor interfaces and surfaces. Reported studies showed that Pt nanowires and PtGe quantum dots like structures are formed on Ge(001) surface [43]. Pyramidal PtGe quantum dot and Pt nanowires can be seen in figure-1.11.

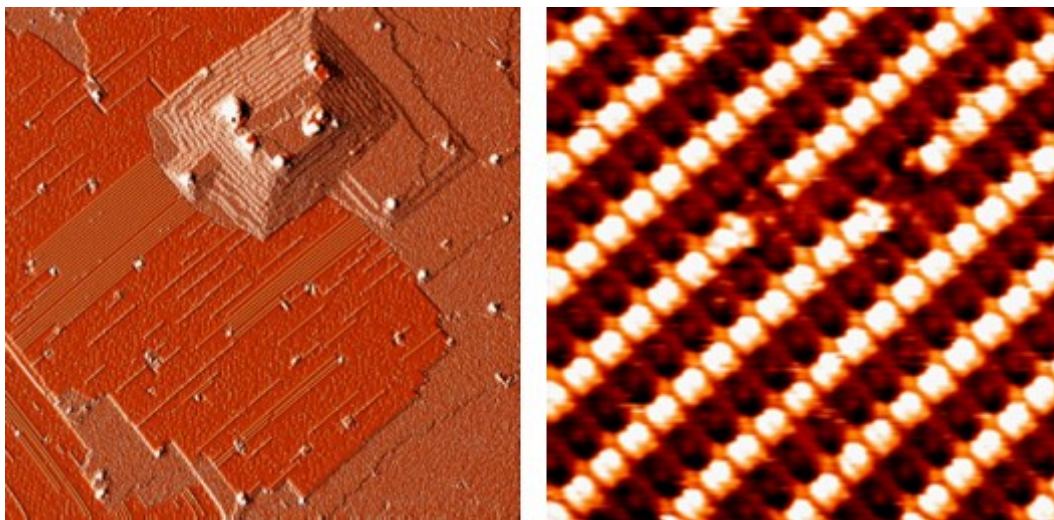


**Figure 1.11** : Metal/semiconductor interfaces and surfaces: (left) STM image (200 nm  $\times$  20 nm) of about 1 ML Pt film annealed on Ge(001) surface. (right) 3 nm  $\times$  3 nm STM image of Pt nanowires on Ge(001) surface, individual Pt atoms can be picked up with an STM tip.

## 2. EXPERIMENTAL

### 2.1 Methods

We need tools to investigate the nature of surfaces at atomic level because human eyes are too poor to observe them. Analytical surface analysis techniques like X-ray photo electron spectroscopy (XPS), low energy ion scattering (LEIS), low energy electron diffraction (LEED), reflected high energy electron diffraction (RHEED) and scanning electron microscopy (SEM) are based on diffraction. X-ray beams (in XPS), ions (in LEIS) and electrons (in LEED, RHEED and SEM) are used as a probe/source to interact with the surface and surface properties are interpreted from the diffracted beams or diffraction patterns or in the case of SEM reflected electrons are interpreted. Although diffraction techniques are quite advanced to study periodic structures and they are sensitive to the surfaces, these techniques are not capable of measuring a single atom structure [4].

With the invention of STM in 1981, observing a single atom became possible. The first STM data by Binnig and Rohrer showed the  $7 \times 7$  reconstruction on Si (111) surface. Before the invention of STM, reconstruction on Si (111) surface was already observed with LEED. Despite the models that were suggested from the LEED measurements, reconstruction on Si(111) surface could only be explained after STM data [3,45].

In case of STM, an atomically sharp tip scans the surface atom by atom. Besides observing a single atom, manipulation on the surface without damaging the surface is also possible with the STM. Although atomic resolution can be achieved with STM, it gives information on both electronic and morphological structure of the surfaces. So, STM data should be analyzed accordingly with great caution.

Self organized structures on the surfaces and interfaces are our main research interests. In such study even the effect of a single atom can not be ignored. Therefore, we did use STM as our main tool to investigate these structures.

### 2.1.1 Scanning Tunneling Microscopy

Scanning tunneling microscope (STM), is a member of scanning probe microscope family (actually can be named as the grandfather), to investigate conductive and semiconductive samples with atomic resolution. It is based on quantum tunneling phenomenon, which explains electron passing through a barrier. Electrons are not allowed to be in a potential barrier but Schrodinger equation has a solution for electrons in both side of the barrier if the potential barrier is thin enough (figure 2.1). This simply implies that electrons can tunnel through the barrier. In case of STM, electrons tunnel between an atomically sharp tip and a conductive/semiconductive sample. Tip or sample is biased with respect to sample or tip to be able to measure a net tunneling current [3,45].

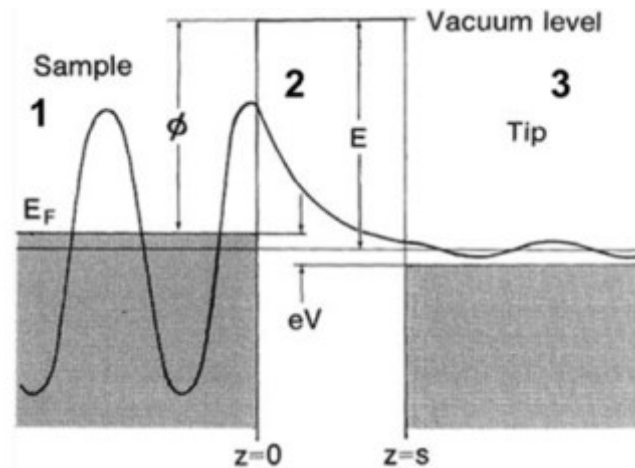


**Figure 2.1 :** Representative image of quantum tunneling from sample to tip.  $\Phi$  is the work function of the sample. Region 2 represents the potential barrier (and in case of the STM it is the gap between the tip and the sample).

In order to make a microscope using the tunneling phenomena afore mentioned tip is scanned over the sample surface while the tunneling current kept constant between the tip and the sample. This mode is called as the constant current mode. While tunneling current is used as feedback parameter, tip-sample distance is varied by the piezoelectric element on which the tip is mounted, so the tunneling current is kept constant. This is achieved by the feedback loop of the STM electronics. As a result, a topographic image of the surface is generated by use of the variance of the voltage applied to the z-piezo element. It has to be mentioned that STM tip follows the morphological and electronic structure of the surface simultaneously. One other mode of STM is the constant height mode where the tip-sample distance is kept constant. In this mode the tunneling changes due to the electronic and

morphological structure of the surface and the measured tunneling current is used to generate a topographic map of the surface.

STM tip can be moved with sub-angstrom resolution by using piezoelectric materials. The resolution is in picometers in the z-direction. Since STM operates at low currents, tunneling current is measured with an I/V (current to voltage) converter. By using an I/V converter, current is converted to voltage depending on the gain factor of I/V converter, preferentially almost immediately after the tip-sample junction [3].

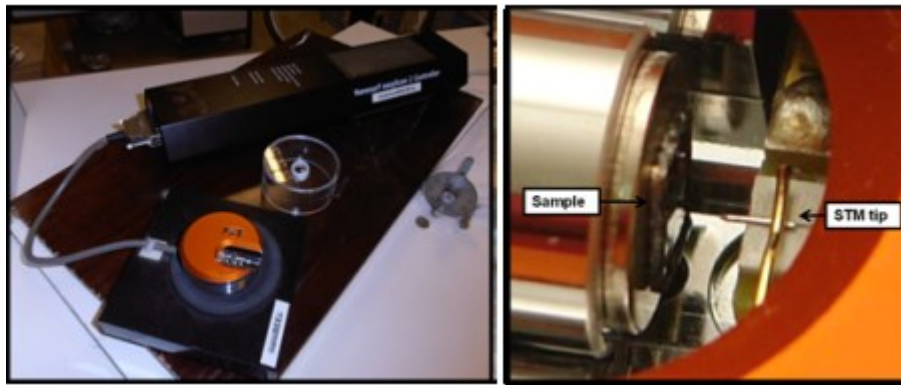


**Figure 2.2 :** STM setup with its electronic and scan head (left) and zoom in on scan head to show sample and tip (right).

STM is a derivative of the electron microscope but with a probe that does not detect the electrons far from the sample but measures the current directly at the probe-sample interface. Although atomic resolution can be achieved by using STM, STM tip actually follows local density of states (LDOS) which electrons are allowed to tunnel. Therefore, interpretation of the STM data is far from being trivial. Ge(001) surface is a good example to explain what STM actually measures. Dimer rows due to the reconstruction are observed on Ge (001) surface instead of atomic resolution.

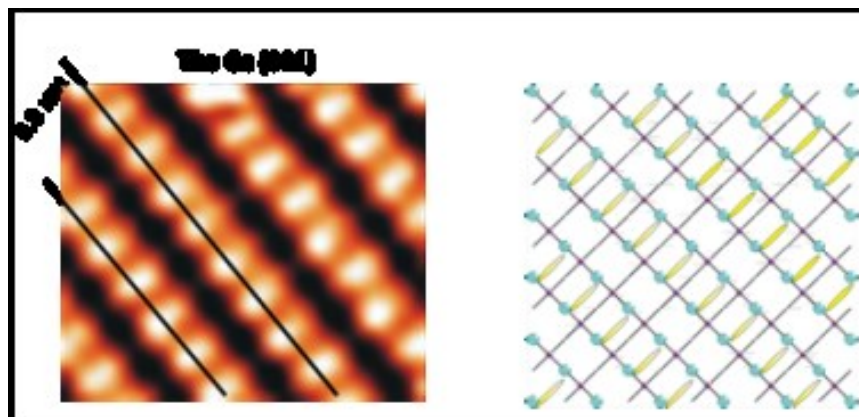


**Figure 2.3 :** STM image of the Ge dimers in filled and empty state to show DOS measurement by STM (left) and its model (right).



Scanning Tunneling Spectroscopy (STS) can be performed by using STM once the feedback loop is disabled. With STS one can basically measure local (tunneling) conductivity between the tip and the sample, which simply gives information on the LDOS of the surface.

A bias sweep is applied and current change due to the bias is measured to have an I-V curve. Differential conductivity can be measured and LDOS can be calculated numerically from measured I-V curves. Proper experiments to investigate electronic and morphological properties of the surfaces can be accomplished by combining STM and STS measurements.

### 2.1.2 Ultra High Vacuum (UHV) and STM

Conductive or semiconductive samples can be investigated with STM but there is another obstacle to study with surfaces. Since we want to investigate the surface properties of the crystals, finding conductive/semiconductive samples is not enough to succeed in STM studies. Samples must be clean and atomically flat. Clean surface means no oxidization, chemical or physical bonding with unwanted molecules or residue on the surface. Although some samples can be studied under ambient conditions owing to their inert surfaces, most surfaces cannot stay clean because of their reactive surfaces or simply due to the ambient humidity [3,4]. Samples like silicon and germanium have reactive surfaces and oxidize immediately under ambient conditions. It is possible to keep these samples clean but to do this ultra-high vacuum (UHV) conditions are needed. UHV is the vacuum level if pressure is lower than  $10^{-9}$  mbar. Ideal gas law is given below.

$$PV = NkT \quad (2.1)$$

with P as pressure, V as volume, N as number of molecules, k as Boltzmann constant and T as temperature. While  $P=10^{-11}$  mbar,  $k=1.38 \times 10^{-23}$  J/K,  $T=300$  K (at room temperature); there are  $2.4 \times 10^{12}$  molecules in  $1 \text{ m}^3$  volume. Gasses in the environment hit to the sample surface continuously and some of them adsorb on surfaces. They can both physisorb or chemisorb on the surfaces. A dosage unit Langmuir (L) is used to explain adsorption mechanism of gasses on surfaces. Assume a surface such that whatever molecule (or atom) hits to it immediately sticks to the surface ( $\theta=1$ ). Such a surface has sticking coefficient of 1. If that surface is dosed with a gas under  $10^{-6}$  mbar pressure for 1 second, than that surface gets covered with 1 layer of atoms (1 mono layer (1 ML)) of that gas just in 1 s. This dose is named as 1 Langmuir (1 L). One layer of atom coverage is called 1 monolayer (1 ML). It is clear that it is not possible to study with a sample under

ambient conditions unless  $\theta=0$ . Basically, that is the reason why UHV is essential for STM studies [4].

UHV systems can be considered as laboratories on their own that provide us specific conditions for experiments. UHV systems are also needed for cleaning and preparation of the sample. Having UHV conditions is an advantage for STM studies but constructing the system and achieving UHV conditions needs patience and caution. First of all specific UHV compatible materials are allowed in UHV studies which have low outgassing under low pressure and at high temperature. Stainless steel, oxygen free copper (OFC), tantalum, molybdenum, alumina, PEEK, polyimide are some of the materials that are allowed to be used in a UHV system.



**Figure 2.4 :** Photo of UHV system on its frame in our laboratory which was constructed during this study.

UHV chamber with tubes and flanges are made by stainless steel (SS304 or SS316) to avoid oxidization. Flanges are produced at standard sizes so it is possible to mount additional parts like STM flange on additional chambers depending on the purpose of the study. OFC gasket is put between two flanges before tightening the flanges with screws so OFC gasket is pressed by the knives-edge of the flanges. Since there is knife-edge on each flange and copper is softer than stainless steel,

knives-edge of the flanges cut into the gasket and achieve leak sealing at very low pressures. Due to the sealing of the connections, UHV can be achieved if the procedure applied properly with right materials. It is not possible to achieve UHV conditions with leaks. Besides finding leaks on full UHV system is not easy.

Studying under UHV conditions has great advantages but it also comes with drawbacks. For example manipulating, moving or mounting a sample under UHV conditions is not as easy as under ambient conditions. Luckily, there are UHV compatible tools for manipulation or transfers in UHV chamber. Magnetic stick is used for linear transfers in UHV chamber. Also manipulator can be added on magnetic stick to transfer and manipulate the sample or tip. BNC connectors can be used to transfer signal or current to inside of the chamber. Voltage or current can be applied in to the UHV systems by using feedthroughs. Moreover, there are rotational or linear feedthroughs by means of which we can achieve rotational or linear motion in UHV studies.

After closing the UHV chamber, vacuum level is the same as the ambient conditions. Gas molecules need to be pumped from the chamber. There are different types of pumps, which can operate at different vacuum levels. Rough pump and turbo pump do active pumping while titanium sublimation pump and ion getter pumps are passive pumps. Rough pump (rotary pump in our case) can operate under ambient conditions and system can be pumped down to  $10^{-4}$  mbar by using the rough pump. Turbo pump can operate from  $10^{-2}$  mbar to  $5 \times 10^{-10}$  mbar. However, there is another obstacle to achieve  $10^{-10}$  mbar. Water adsorbed on the inner walls of the UHV chamber under  $10^{-8}$  mbar pressure cannot be pumped in a reasonable time from the chamber. Therefore the chamber needs to be literally baked by heating up to  $120^\circ\text{C}$  to get rid of the water. UHV chamber can be put into an oven or wrapped by heating ribbons for baking. Rough and turbo pumps operate during baking. Base pressure first increases during baking and in time passive pumps are allowed to operate continuously and the pressure drops down below  $1 \times 10^{-9}$  mbar. Titanium can be sublimated by using titanium filaments (Ti Sublimation Pump (TSP)) and  $\text{H}_2$  can be gathered on Ti coated walls of the TSP with the help of ion gather (IG) pump. Actually, in our system Turbo molecular pump can pump the system down to  $5 \times 10^{-10}$  mbar after baking. However the  $\text{H}_2$  cannot be easily pumped by the Turbo pump. In addition, we cannot let the turbo pump run during STM measurements due to the vibrational noise. Therefore, we need the passive pumps like the IG pump and the TSP. TSP simply gets the ions (especially Hydrogen) on the walls of the chamber. The ion getter pumps work differently. The



IG pump has plates on to which we apply +3 kV. The pump has strong magnets outside its walls. The high voltage on the plates causes the molecules in the chamber to polarize and when they touch the plates of the IG pump, they lose at least one electron. Since they become (+) charged, the pump plates repel them. Due to the large magnetic field, they move on a spiral and crash on the Ti coated walls of the inner chamber and get stuck there. This reduces the pressure. Also this way the system pressure can be kept below  $5 \times 10^{-10}$  mbar even without the turbo molecular pump. Nevertheless, we must sublime Ti to refresh the inner walls of the chamber once in a while.

Since STM is very sensitive to vibrational noise, damping to reduce the noise is essential after achieving working condition for the STM. Concerning STM, even minute vibrations end up in a tip crash. First step is to turn off the active pumps, only ion gather pump is allowed while STM is operational. Second step is to reduce the vibration by isolating the UHV system by using an active vibration isolation system. Commercial systems can be found for system isolation. Due to the design of the STM, isolating the STM head from UHV chamber is the third step.

## 2.2 Experimental Set Ups and Sample Preparation Techniques

### 2.2.1 Nanosurf EasyScan STM 2

Nanosurf Easyscan STM 2 is considered for student labs to improve student experience in STM studies. It is compact system and it has a small control electronics unit and an STM head. It is also stable for advanced research studies. By use of this set up the morphological and electronic properties of conductive/semiconductive samples under ambient conditions can be studied.

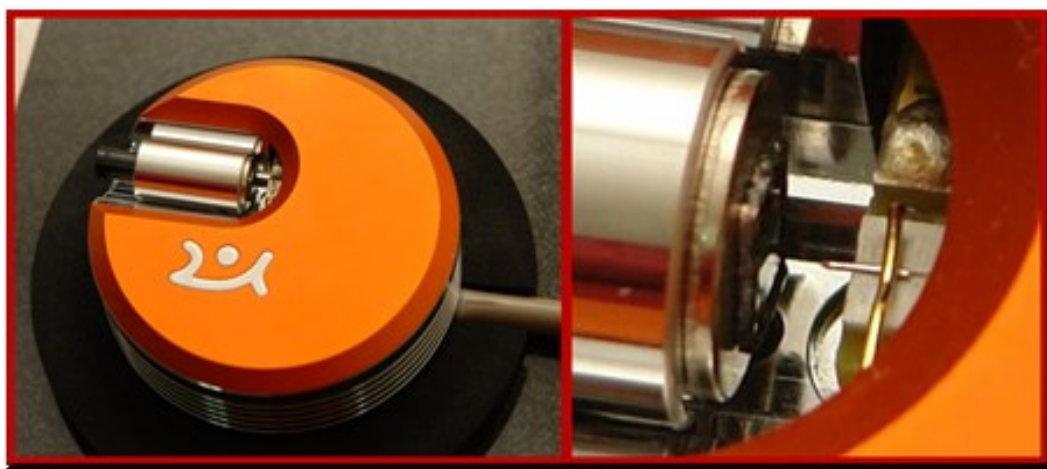


**Figure 2.5 :** Nanosurf Easyscan STM head with sample and tip.

Software of Nanosurf Easyscan STM has a user-friendly interface. Mounting/unmounting the sample and the tip is relatively easier than UHV STM (figure-2.5). This simplicity allows us to change samples quickly. Cylindrical sample holder with sample on it is placed on piezo and approached to the tip by slip-stick motion of the piezo. Sample approach is computer controlled and as a result, approach is fast. Moreover, this ease of study makes the accessible amount of data incredibly large. In one day, more than five different samples can be scanned at many different tunneling zones.

Maximum scanning area is  $600\text{ nm} \times 600\text{ nm}$  with this system. Nanosurf Easyscan STM 2 is a tip biased system and it can be operated at constant current mode. Gain factor of its I/V converter is  $10^8$ . I/V (current/voltage) and I/Z (current/distance) curves can be obtained by performing scanning tunneling spectroscopy (STS) on a point, line or grid. 0.25 mm diameter  $\text{Pt}_{80}\text{Ir}_{20}$  wires are used as an STM tip after prepared with mechanical cutting.

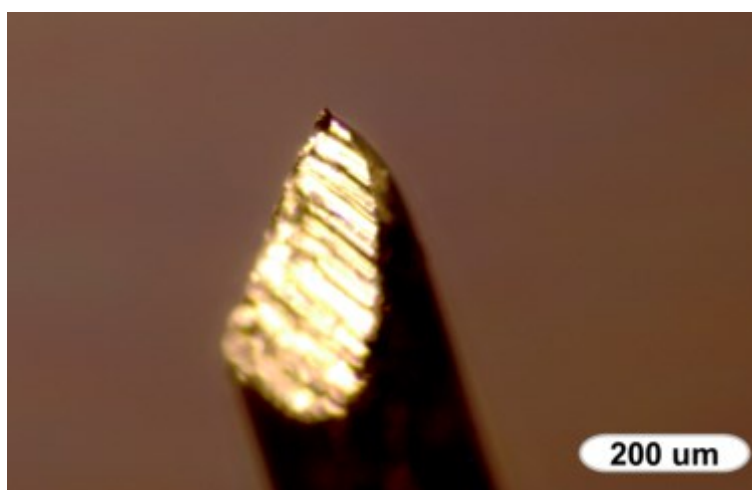


**Figure 2.6 :** Optical image of mechanically cut  $\text{Pt}_{80}\text{Ir}_{20}$  tip.

### **2.2.2 Ultra High Vacuum Scanning Tunneling Microscope (UHV-STM)**

UHV-STM should be mentioned as a complete system with UHV chamber, STM and additional parts of the system like evaporators and sample manipulator.

UHV system that we constructed in our laboratory operates below  $5 \times 10^{-10}$  mbar. Surely there were commercial parts of the system like feedthroughs, magnetic sticks, flanges, tubes and vibration isolation legs. Some important parts of UHV system such as heating ribbons, platinum (Pt) evaporator, sample carrier, and electrical connections for sample manipulation were homemade by necessity.



**Figure 2.7 :** Additional homemade parts of UHV system. Sample fork (upper images), Pt evaporator (middle) and sample carrier (bottom).

Also an aluminum frame as a vibration isolation table was constructed in the laboratory because of the low budget by using six meters aluminum profiles.

Some parts like the ion pump, high voltage source (for ion pump), high voltage cable, sputtering system and STM were donated from different research institutes around the Europe.



**Figure 2.8 :** Making the vibration isolation table. Preparation of the isolation system (upper images), drawing of the table (bottom-left) and the table itself (bottom-right)

Rough pump that was mounted on our system was a rotary pump from Oerlikon-Trivac. We used an Oerlikon SL300 turbo molecular pump. Titanium sublimation pump was embedded in our ion gather pump so we were also able to evaporate titanium to increase the capacity of ion gather pump. By following the procedure, UHV conditions were achieved and  $5 \times 10^{-10}$  mbar were measured on ion gauge, which was its measurement limit. Pumps on the system are shown in figure 2.9.

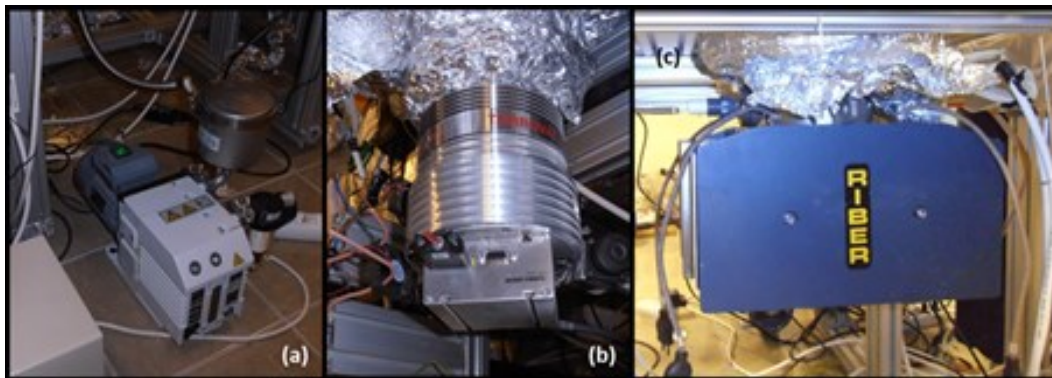


**Figure 2.9 :** Pumps of UHV system. Rough pump, turbo pump, ion pump (in order from left to right).



Our UHV-STM was donated from Twente University and was designed with a manual lever-type approach mechanism. Electrical connections of an STM was through the BNC connectors.

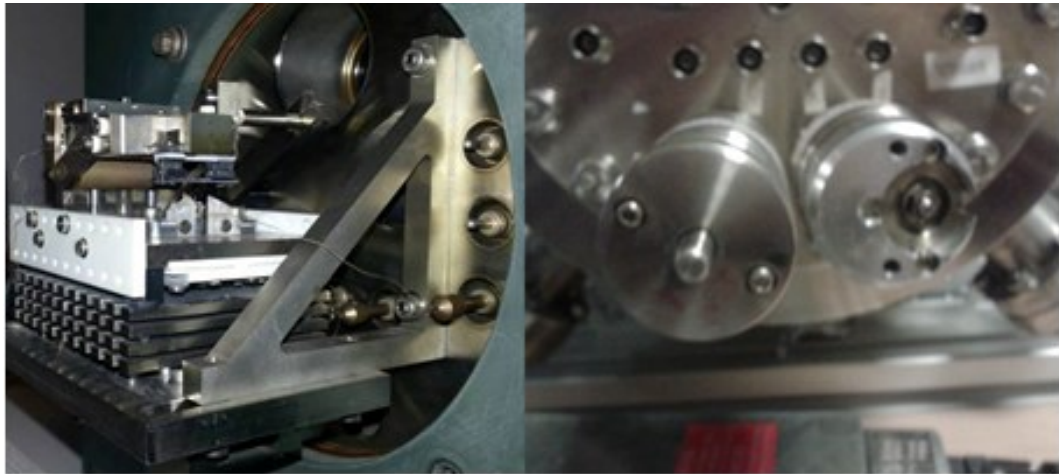


**Figure 2.10 :** UHV STM head (left) and linear and rotational feedthroughs (right). Tip was mounted on scanning piezo that was placed between two sapphire blocks. Sapphire blocks support the sample after coarse approach.

A worm gear and rotational feed-through were used in the approach mechanism. The sample sits on a head which is supported with a wormgear. After the sample was mounted on the STM head the wormgear is rotated and the sample lands on the sapphire legs. After this point, as the worm gear was rotated more, the sample which is supported by the sapphire legs slowly approached the tip as the third support is simply the worm gear itself. This way the manual rotation is translated to a linear motion and the sample approached the tip. Sample was approached and tunneling was done mechanically manually with the help of a rotational feedthrough (see Appendix A).

Concerning the approaching by rotational feedthrough; one turn on the outside translated to 100  $\mu\text{m}$  linear motion of the sample towards the tip and tunneling must be reached in maximum 15 turns.

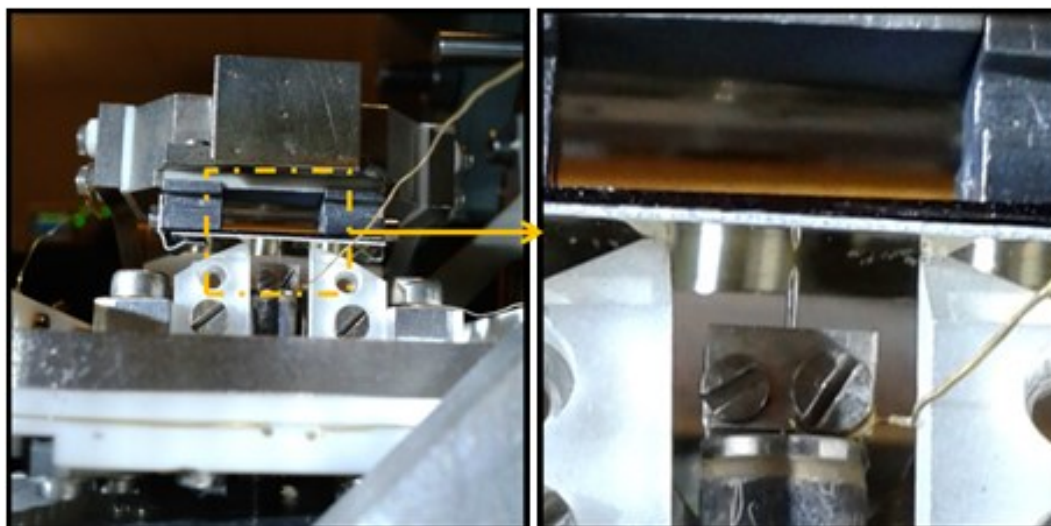


**Figure 2.11 :** UHV STM head (left) and zoom in on tip-sample (right).

During this study a NANONIS STM control unit was purchased and used to control the UHV-STM. A Femto GmbH. I/V converter was used between the STM and the electronic. Gain factor of the I/V converter was adjusted to  $10^9$  in all UHV-STM studies. Up to a  $200 \text{ nm} \times 200 \text{ nm}$  area can be scanned by using this STM and the control electronics.



**Figure 2.12 :** On the left image, NANONIS STM control unit and UHV system behind it. Femto I/V converter is on the right image.

UHV-STM and NANONIS control unit was tested with gold (Au) sample under ambient conditions. The system worked properly and 150 nm thick polycrystalline gold surface was scanned with UHV-STM. STM data shown in figure 2.13 shows the rough Au surface.

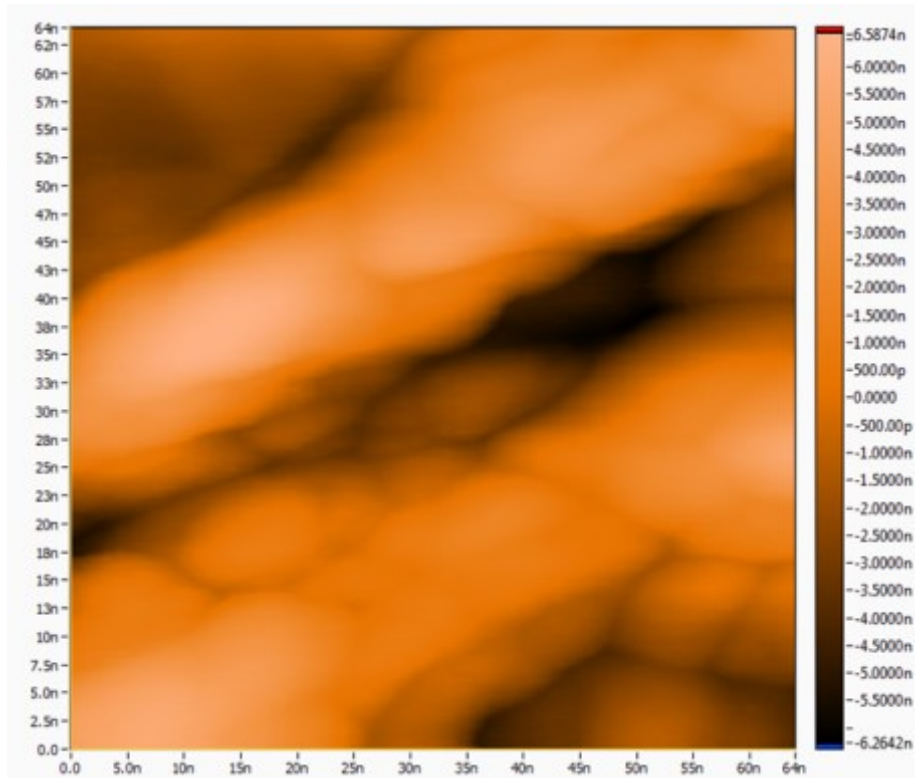


**Figure 2.13 :** STM image of rough Au surface with UHV-STM and NANONIS control electronic. Image size 64 nm × 64 nm,  $I = 0.2$  nA,  $V = 100$  mV. Measurement was done under ambient conditions.

### 2.2.3 Ion Irradiation Facility (France)

We prepared some samples at İTÜ and sent them to EMIR network of France. HOPG crystals were irradiated by swift heavy ions (SHI) in Large Heavy Ion National Accelerator (Grand Accélérateur National d'Ions Lourds - GANIL) facility [46].

## 2.3 Samples and Sample Preparation

Sample preparation is important as well as investigating the samples with advanced techniques. Applying the correct preparation method and keeping the samples clean during and after preparation definitely improves research quality. More importantly all samples are not suitable for cleaning with the same technique.

### 2.3.1 Dropcast Method for Preparation of Moiré Structures on HOPG

Dropcast method was used to prepare moiré samples under ambient conditions. Various chemicals were dropcasted on clean HOPG surface by automatic micropipette. Disposable tips were used and they were cleaned with same chemical

before use. HOPG crystals were cleaved by using scotch tape and chemicals were dropcasted on fresh surface. Chemicals and results will be discussed later.

### 2.3.2 Cleaving Highly Oriented Pyrolytic Graphite (HOPG)

This method was used to have clean surface on layered crystals by peeling the topmost layers with the help of a sticky tape.

Highly Oriented Pyrolytic Graphite (HOPG) was our main crystal as a calibration sample for STM studies and as a source of moiré samples. HOPG was cleaved by using scotch tape because of its layered structure and weak van der Waals interaction between the layers. We used HOPG for calibration and preparation of moiré structures after having fresh and clean surface by cleaving the crystal. The procedure was applied under ambient conditions. The tape is gently pushed on the HOPG surface and slowly pulled. The result is shown in figure-2.14.

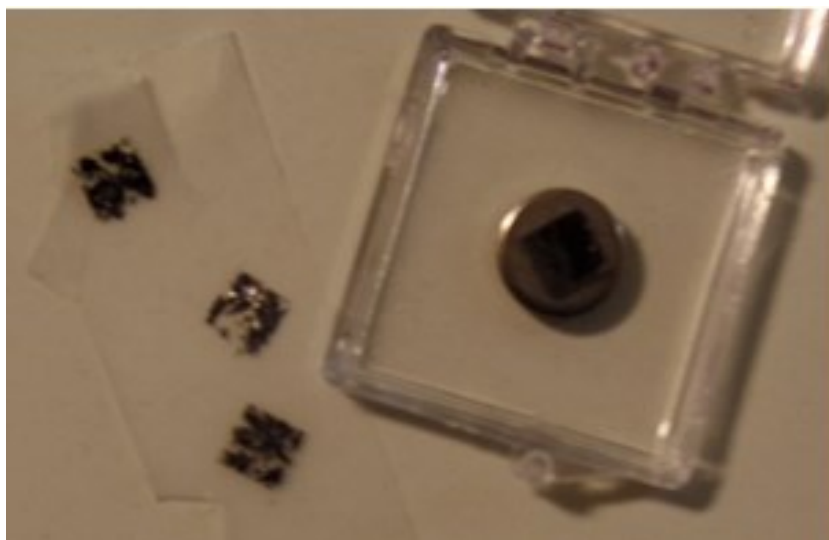


**Figure 2.14 :** Cleaved HOPG crystal. Topmost layers of HOPG crystal was peeled off by scotch tape. Several stick-and-pull procedures were applied as seen on the tape (to the left).

### 2.3.3 Cleaving and UHV Preparation of Ge(001)

Ge(001) wafers used in this study were nearly intrinsic 375  $\mu\text{m}$  thick 2 inch Ge(001) wafers. 22 mm  $\times$  8 mm crystal was obtained by cleaving the wafer. Crystal was handled with zirconia tweezers to avoid metal contamination. Diamond pen was used to notch the edge of the wafer. After that, with applying gentle pressure near the notch, the crystal wafer was cleaved into two pieces. Then the cleaving procedure was reapplied until we got the needed size.  $\text{N}_2$  gas was blown on the Ge(001) piece to get rid of the dust caused by notching and cleaving. Ge piece was



mounted on the UHV-STM sample holder and further cleaning was not applied under ambient conditions. So the sample was mounted in UHV system.

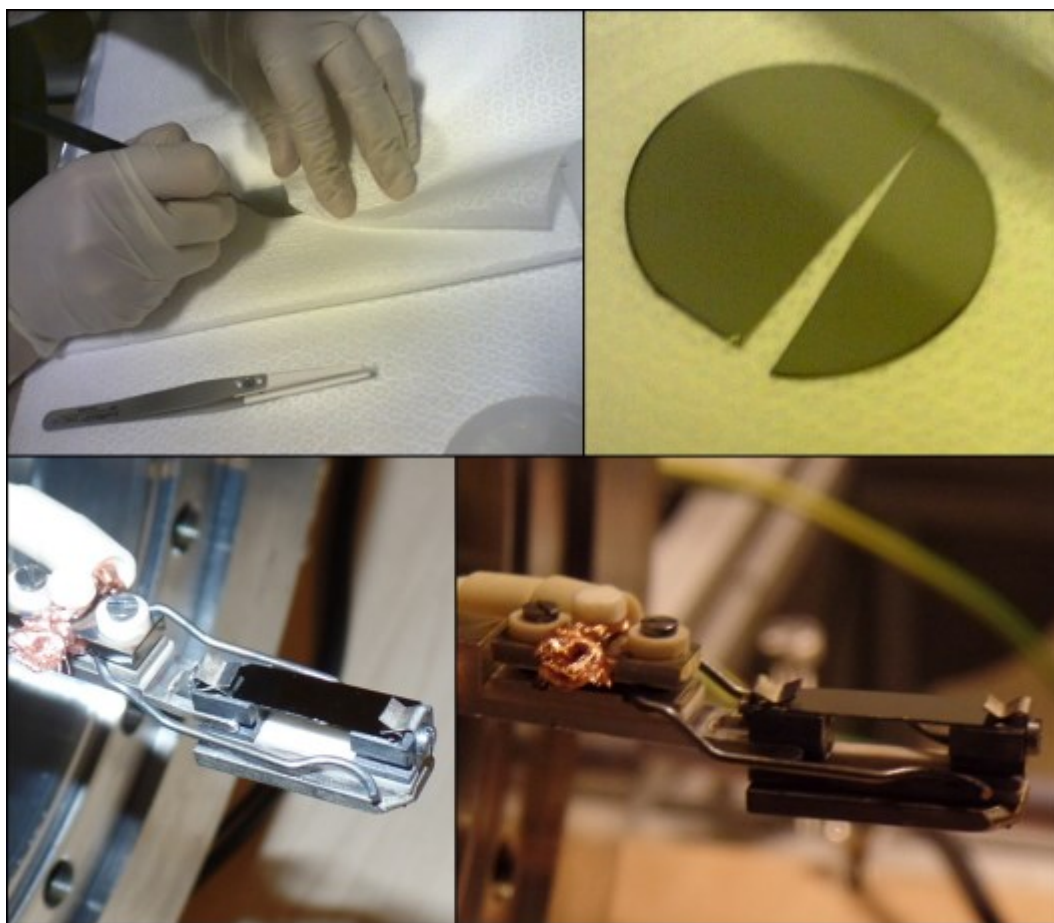


**Figure 2.15 :** Ge cleaving by diamond pen (upper left image), cleaved Ge crystal (upper right image) and mounted on sample holder on the fork (bottom images).

Moreover sample holder parts were designed in this study. Their desing pictures are given in figure 2.16

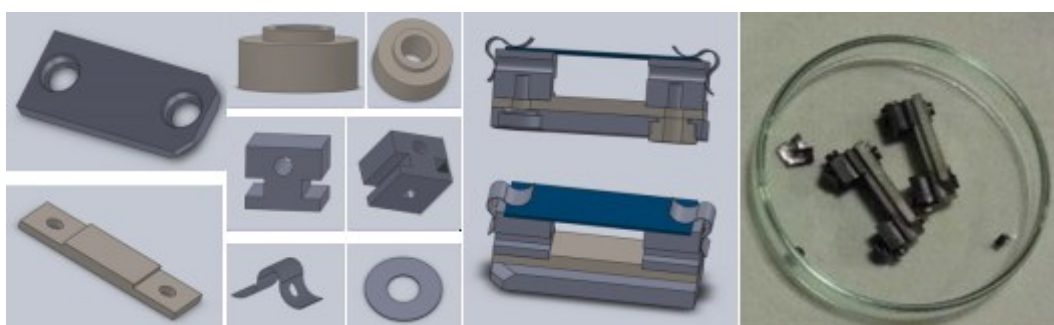


**Figure 2.16 :** Designed parts (left) and assembly (middle) of sample holder on the left side. Two assembled sample holders.

As soon as UHV conditions were achieved, Ge (001) crystal was heated by direct current heating. Current was increased slowly while keeping the pressure below 2

$\times 10^{-9}$  mbar. Current/temperature curve of previous studies were used as a reference. Sample was slowly heated up to 900K; at the same time pressure kept at  $1 \times 10^{-9}$  mbar. Same procedure was applied for 10 days to degas the sample, holder, finally 5 A current was applied to reach 900 K; the sample radiated dark red at that temperature for 24 hours.

Sample was sputtered after degassing and cooling down to room temperature. Following sputtering, the sample was annealed again by applying 5 A to reach 900 K. The sample was flashed more than 30 times after sputtering by increasing current to 12 A and decreasing to 5A. Sputtering-degassing-flashing cycle was repeated 3 times. Sample was at room temperature at the beginning of each cycle.

#### **2.3.4 Swift Heavy Ion (SHI) Irradiation**

Swift heavy ion (SHI) irradiation is an interest of fundamental and applied physics research. Ions are accelerated at high energies and different ion beams are available. During irradiation process, electron stopping is dominated over nucleon stopping if the ions are SHI. Ion tracks are produced due to irradiation and atomic reconstruction is also possible to occur [40-42].

Large Heavy Ion National Accelerator (Grand Accélérateur National d'Ions Lourds - GANIL) facility was used for swift heavy ion (SHI) irradiation.  $^{238}\text{U}^{31+}$  ions were used in SHI irradiation process and irradiation energy was 109 MeV.

HOPG crystals were irradiated by SHI to see the effect of defect formation on the surface morphology and electronic structure. HOPG crystals were supplied from Goodfellow and SPI companies. Also, moiré samples were irradiated by SHI.

### 3. HOPG – MOIRÉ SYSTEM

We studied on these structures by scanning tunneling microscopy (STM) and spectroscopy (STS). To work with these structures, samples were needed to be prepared properly. Proposed and applied chemical methods always require time and extended processes (ref.). Moreover, the crystal may be damaged because of the chemical and mechanical processes applied.

We have discovered that simply by drop casting cyclohexane on to HOPG surfaces (SPI™ grade 2 and 3) and letting the samples dry in a dust free and dry environment (simply in a desiccator) many different moiré structures can be obtained on the surfaces. Pure and fresh (VWR™ cyclohexane, HPLC grade) is used for each sample preparation. We have checked the HOPG surfaces by means of micro Raman spectroscopy for probable contamination or residue from the cyclohexane drop casting and drying method. Figure 3.1 shows the micro-Raman spectrum obtained on the cyclohexane solution and cyclohexane dropcasted HOPG surface. The HOPG samples were thoroughly investigated prior to cyclohexane drop casting by STM.

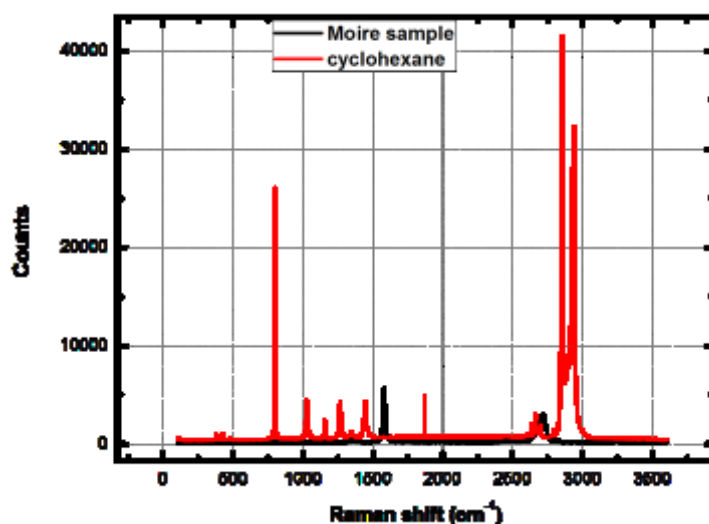


**Figure 3.1 :** Raman spectrum of cyclohexane dropcasted HOPG surface and cyclohexane solution. The moiré sample only shows the peaks intrinsic to the HOPG surface.

Rarely (1 in 50 tunneling zones) native moiré patterns were observed on both grades 2 and grade 3 HOPG surfaces. Within this study, we also used different solvents to see their effects on HOPG samples and the same drop casting and drying procedure were applied with n-hexane, chloroform and toluene. As a result, moiré patterns were observed on every sample that was prepared with cyclohexane. Other chemicals were not effective to produce them so we decided to continue our study with cyclohexane. Used chemicals and geometric moiré periodicities shown in figure-3.2.

Used Chemicals	Result
Hexane	GMP(nm): 6.53 & 2.9
Isopropanol	No moiré
KOH solution	No moiré
Chloroform	Not clear
Cyclo-hexane	GMP (nm): 3.30, 12, 7, 1.8, 3, 3.8, 3.37, 3.63, 2.54, 2.48, 7.61, 3.42, 3.56, 28.95, 3.65
toluene	GMP (nm): 1.6

**Figure 3.2 :** List of used chemicals in preparation of moiré structures on HOPG. Observed periodicities were added to compare the effect of each chemical.

The formation of super-periodic structures on HOPG was found to dependent on the chemical used. Only after treatment with cyclohexane, in every tunneling region we encountered moiré patterns with geometric moiré periodicities (GMP) from 2.48 nm to 28.95 nm. All the measurements reported here were performed under ambient conditions. The experimental conditions were carefully controlled and several consistency checklists were developed. Many different moiré samples were prepared and investigated by use of different tips (more than 100 samples and 150 tips were employed during this study with in the past years). The measurements

were extensive in order to eliminate the possible tip effects, noise or possible artificial structures due to measurement conditions. On the same sample, reliable and consistent measurements for longer than a week were possible.

After improving the preparation method, we observed both moiré patterns and atomic resolution on the pattern under ambient conditions with STM. Concerning the STM measurement, to achieve atomic resolution on moiré structures were easier than on HOPG. HOPG has smooth surface but definitely the surface is not flat so maybe moiré patterned areas are flatter than pristine HOPG surface.

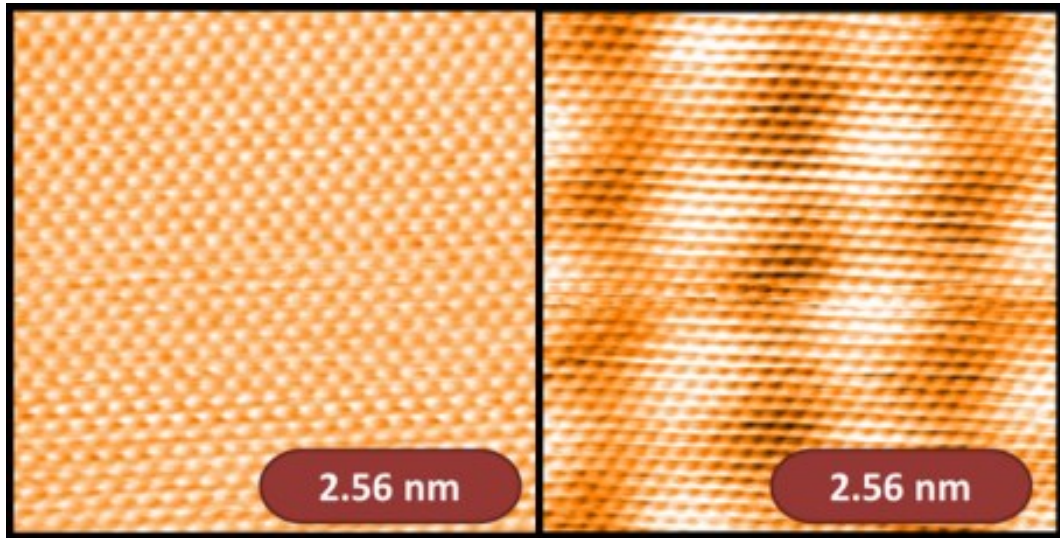


**Figure 3.3** : Atomic resolution on HOPG (left) and on moiré structure (right). Tunneling parameters  $I = 0.5$  nA,  $V_b = -50$  mV. GMP = 1.6 nm.

On HOPG surface it is possible to get atomic level resolution (where one sees the triangular lattice with only the  $\beta$  site atoms) only around 50 mV tunnel junction bias. At higher biases, atomic resolution vanishes on clean HOPG surface. Intriguingly, the atomic resolution (triangular or hexagonal) was achieved at higher biases on moiré regions, as high as 800mV. Atomic resolution on moiré pattern at high bias is shown in figure-3.4. Tip stability was checked by observing atomic resolution on clean HOPG area just next to moiré pattern. Since we observed triangular atomic resolution on the clean HOPG terrace around 50mV tunnel junction bias just next to the moiré patterned area we can safely state that the tunnel junction was essentially stable.



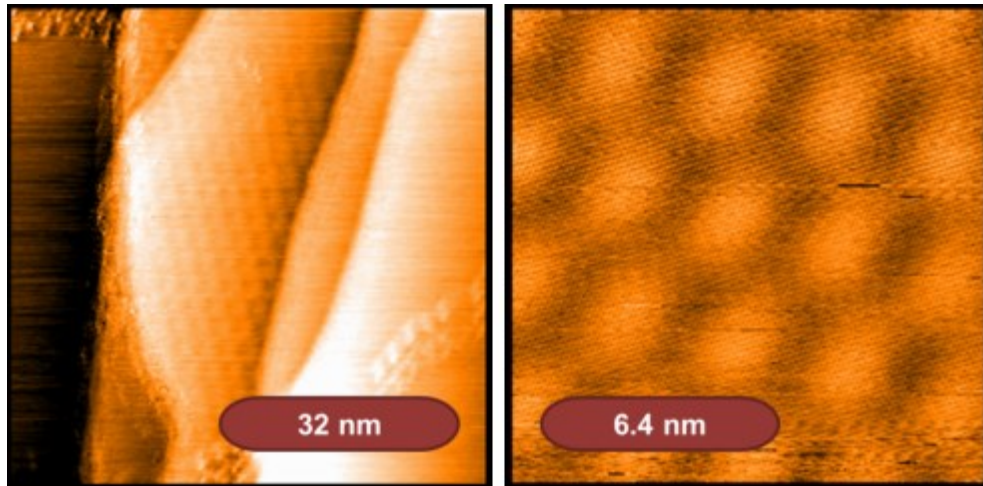


**Figure 3.4 :** STM image of moiré structure in large area on the left ( $I = 0.5$  nA,  $V = -200$  mV). Zoom in STM image on the boundary of the moiré structure with atomic resolution at high bias (right) ( $I = 0.5$  nA,  $V_b = -500$  mV).

In STM studies, observed structures may change due to tunneling current or bias. These changes can be checked by performing poor man's spectroscopy with an STM. In this study, bias depended poor man's spectroscopy was performed on moiré structures by keeping tunneling constant and scanning the same surface zone with different biases. Corrugations of observed structures were acquired from the line scans on these structures. Because moiré patterns have triangular structure, line scans were taken in three directions and average corrugation ( $h$ ) was calculated from the lines. Each line was taken three times to calculate the average corrugation.

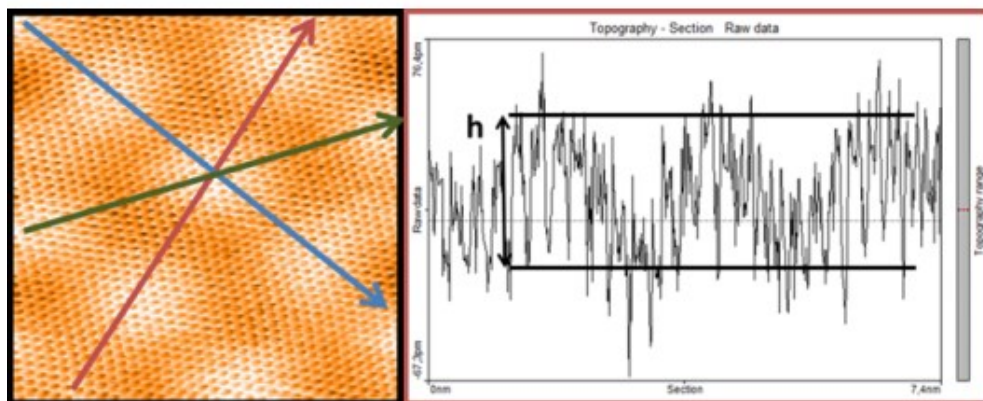


**Figure 3.5 :** Corrugation analyses of moiré structure. (STM image of moiré pattern with atomic resolution and line scans on each direction of the pattern on the left ( $I = 0.5$  nA,  $V_b = -45$  mV, GMP = 2.54 nm).

Most intriguingly, **contrary to previous reports, we observed that the apparent corrugations in STM images of moiré patterns change as a function of tunnel junction bias**, and these changes on various moiré structures do not occur in a monotonic fashion. A simple geometric investigation of the atomic structure of the

moiré patterns revealed that different atomic moiré periodicities result in similar geometric moiré periods, which bring forth the importance of information on the real atomic structure (RMP) of each moiré pattern observed in STM images. This GMP vs. RMP discussion was made in the previous chapter.

Figure-3.6 shows the variation of the apparent moiré corrugations observed on three different moiré patterns (with different GMPs) as a function of the tunnel junction bias. We also show that the atomic resolution is observable in a broad range of biases on this moiré pattern. Decreasing corrugation with increasing bias was observed for these three super-periodic structures. Measured GMPs of these structures were 2.54nm, 3.45nm and 12nm.

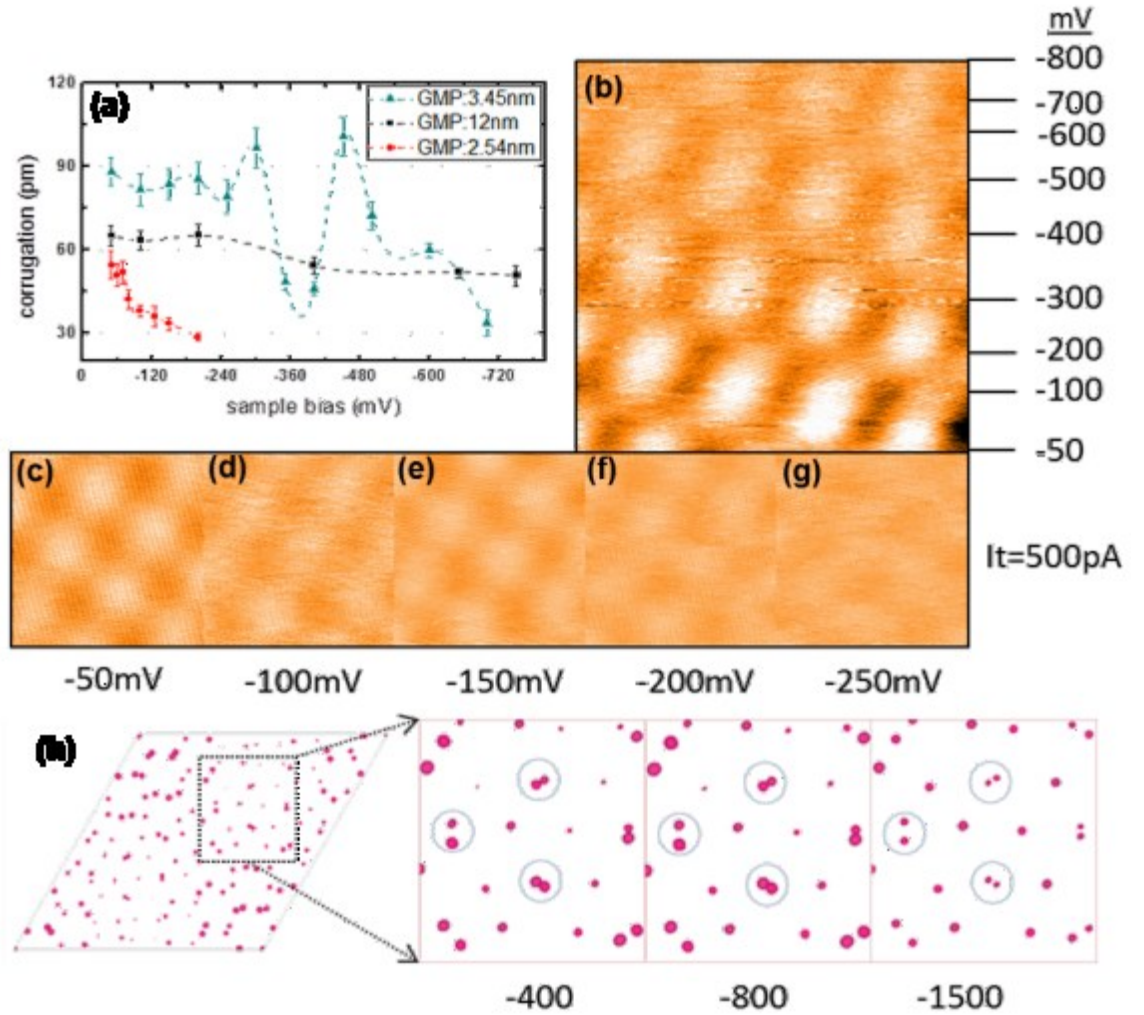


**Figure 3.6 :** (a) Curves of corrugation change with respect to bias (three different moiré patterns). (b) STM image of moiré pattern. Bias was changed from -50 mV to -800 mV during scanning. (c) - (g) STM images of the same moiré pattern with different bias. (h) Charge plot of calculated DOS of moiré unit cell (GMP=1.6 nm, RMP = 2.84) (Theoretical calculations were done on moire systems, please see the Appendix B).

While observed corrugation of two samples decreased with increasing tunneling bias, the third sample did not show only a decrease but also varying behavior (both increasing and decreasing) as a function of increasing bias (figure 3.6-a). These variations may indicate different electronic states on moiré structures. Oscillating behavior due to the bias was also observed charge plots of calculated moiré unit cell (figure 3.6-h).

Besides the corrugation change due to the increasing tunnel junction bias, contrast reversal on moiré patterns were also observed on sequential scanning of the same area with the same scanning parameters with STM (figure 3.7). Consistency checks on tip stability were made by achieving atomic resolution and performing STS on clean area. Contrast reversal on such giant structure shows the electronic behavior of these structures.

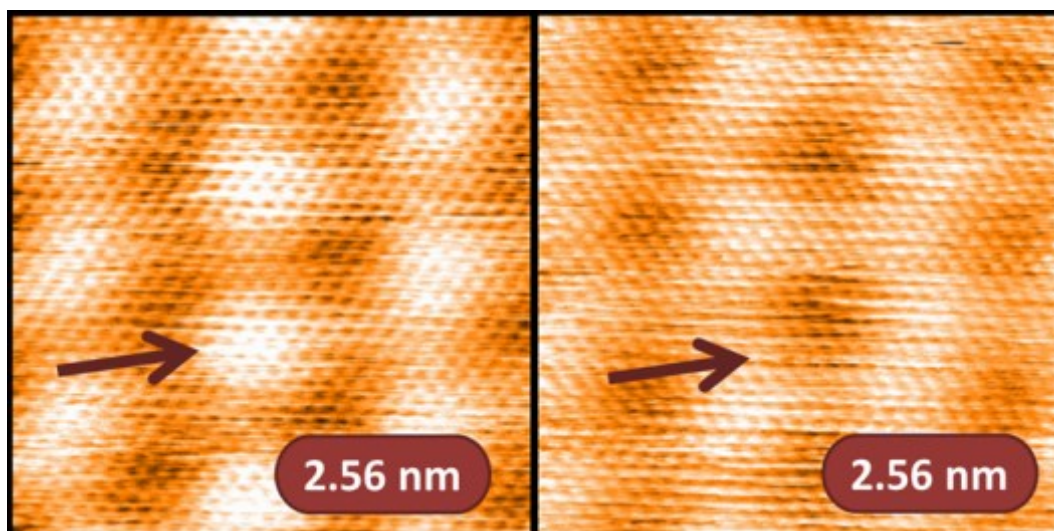


**Figure 3.7 :** STM images of moiré pattern with atomic resolution. Left image was typical STM image of moiré pattern with atomic resolution. STM image on the right shows contrast reversal on moiré structure, triangular structure switched to hexagonal during STM study. And bright moiré spots became dark. Scanning parameters were  $I=0.4$  nA,  $V_b=-50$  mV, GMP = 1.6 nm.

Such corrugation changes can be considered as tip effect but since we could continue STM measurements without any problem and as the tip was checked by achieving atomic resolution after having this image, we speculate that this is due to the intrinsic electronic nature of the moiré pattern. Moreover, a reported study supports our idea on contrast reversal. Although origin of moiré pattern was different (moiré pattern on graphene/Ir(111) surface), it was stated that the contrast reversal is possible to observe at different bias voltage by using STM [39]. In our



case, even if we did not change the scanning parameters, STM tip might shift between two electronic states.

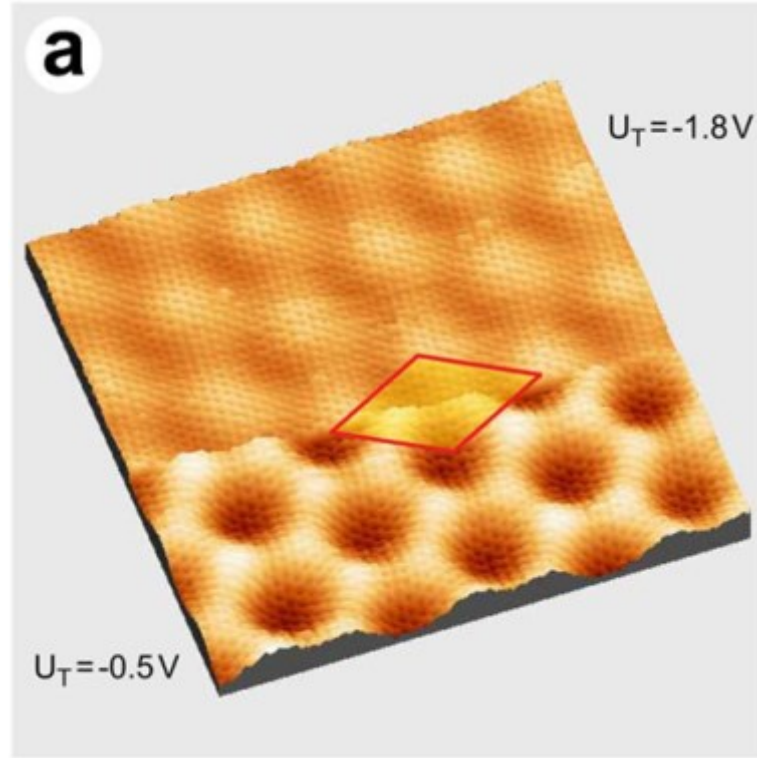


**Figure 3.8 :** STM image of contrast reversal on moiré pattern on graphene/Ir(111) system. ( $I = 15 \text{ nA}$  and  $V_b$  changed from  $-0.5 \text{ V}$  to  $-1.8 \text{ V}$ ) [39].

After STM studies, moiré structures were investigated by scanning tunneling spectroscopy (STS). Scanning tunneling spectroscopy (STS) was performed on moiré patterns and on pristine HOPG surfaces. Tunneling current was measured during bias sweep with disabled feedback loop. Since the feedback loop was disabled, tunneling current changed due to the bias. Tunneling current depending on the bias ( $I/V$ ) curve was obtained. Because of the tunneling parameters, tip-sample distance may be different for each experiment. To prevent the effect of initial parameters like tunneling current and tunnel junction bias, local density of states / bias (LDOS/ $V$ ) curves were derived from measured  $I/V$  curves to compare the difference between HOPG and moiré structures.

Figure 3.9 shows the LDOS/ $V$  curves on pristine HOPG and on two moiré structures with  $1.8 \text{ nm}$  and  $1.6 \text{ nm}$  GMP. Clearly, moiré structures were more metallic than HOPG. With the help of ab initio calculation, we can state that the shoulders between  $-0.5 \text{ V}$  and  $-1.0 \text{ V}$  on LDOS curves of moiré structures indicate van Hove singularities.

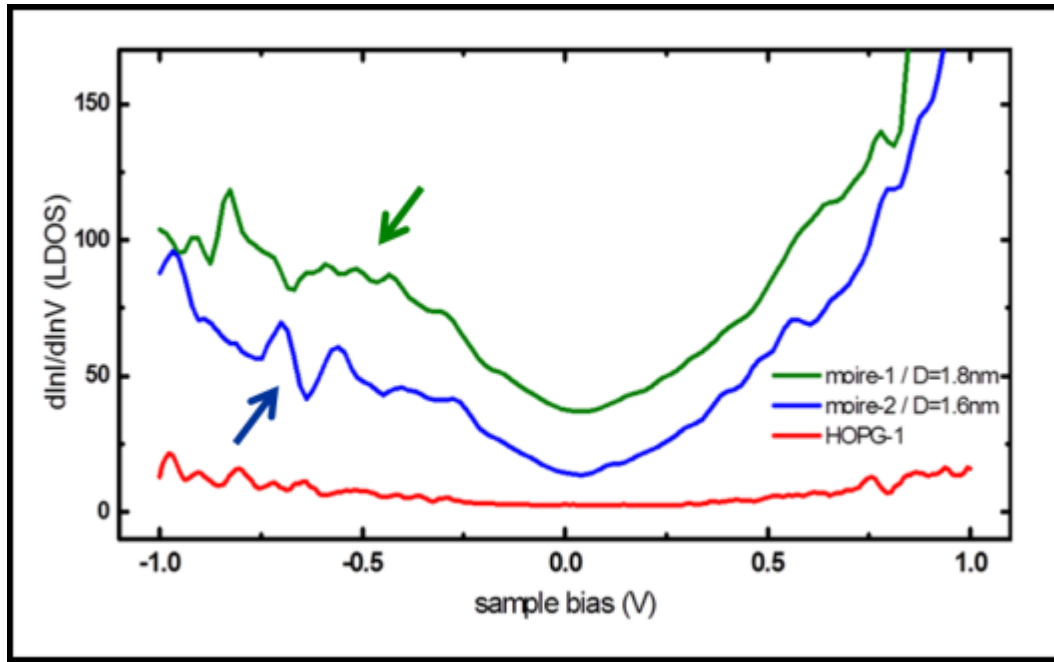


**Figure 3.9** : LDOS curves of HOPG and moiré patterns on HOPG (GMP of the patterns were 1.6 nm and 1.8 nm)) system. Arrows points the shoulders due to the van Hove singularity. (See Appendix B for theoretical calculations).

In summary, we improved the methodology to produce moiré patterns on HOPG surfaces, we studied their atomic structure and we have seen that not all of the similar appearing moiré patterns with same periods have the same atomic substructure. So we introduced the RMP and GMP concepts in this study. We have also shown for the first time that apparent corrugation of moiré patterns do change as a function of tunnel junction bias on some moiré patterns. During this study, we have started collaboration with a theory group and confirmed our results theoretically. Our STS results also clearly showed that moiré structures behave more metallic than HOPG surface. And above all we have shown that all these measurements and analysis can be conducted under ambient conditions.

#### 4. IRRADIATED HOPG AND MOIRE

In this study we also focused on the defect formation due to  $^{238}\text{U}^{31+}$  irradiation on HOPG samples (from different suppliers) and moiré samples. HOPG crystals were provided from SPI<sup>TM</sup> and Goodfellow; crystals from both SPI and Goodfellow were used in HOPG studies but moiré structures were prepared only on SPI-HOPG crystals.

Pre irradiation study was made in our laboratory by using STM to compare the effect of SHI irradiation defects and changes on surface structure after the irradiation. In addition, moiré structures were checked by STM before irradiation to be sure that moiré structures were there to be irradiated. Samples were sent to CNRS for irradiation and irradiated by  $^{238}\text{U}^{31+}$  ions with 10<sup>9</sup>MeV irradiation energy. SHI source and irradiation energy were the same for Goodfellow and SPI crystals but the flux was different. Goodfellow-HOPG samples were irradiated with  $1 \times 10^{10} \text{ cm}^{-2}$  flux. Flux was  $3 \times 10^9 \text{ cm}^{-2}$  for SPI-HOPG crystals. Samples were studied by STM after the irradiation.

Fist of all it should be mentioned that we did not observe any defects on some tunneling zones. When we observed the defects, morphology of the surface was like clean HOPG surface on large are scanning as it can be seen in figure 4.1. We counted irradiation defects on 204.8 nm × 204.8 nm area on Goodfellow-HOPG. Considering the flux ( $1 \times 10^{10} \text{ cm}^{-2}$ ), four irradiation defects should have been observed on that area but we counted three of them. So we considered that the irradiation was not uniform. This might be the reason why the observed flux was less (or for some measurement more) than the irradiation flux.

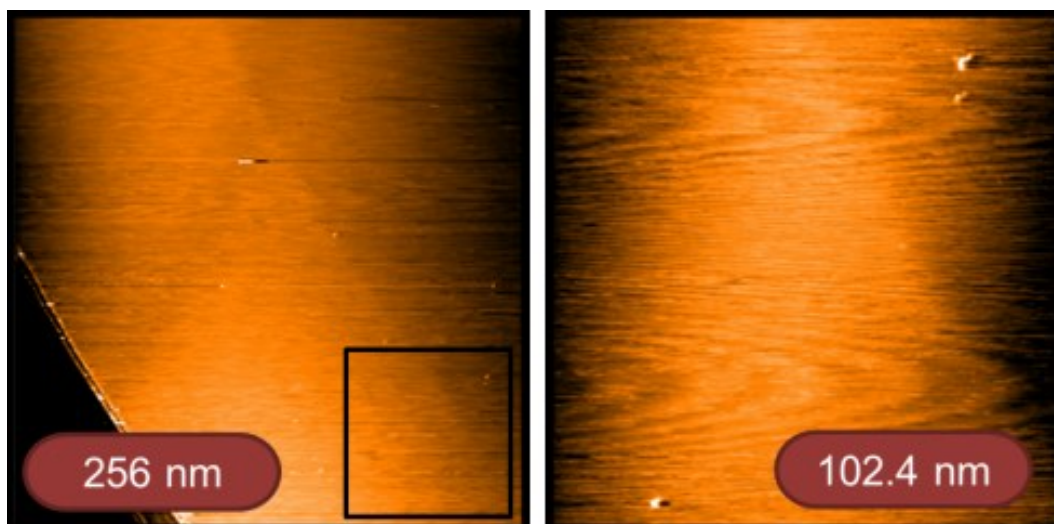


**Figure 4.1 :** STM image of SHI irradiated Goodfellow-HOPG surface in large scale (left) ( $I = 0.4$  nA,  $V = -75$  mV). STM image on the left shows HOPG surface with irradiation defects ( $I = 0.3$  nA,  $V = -100$  mV).

After finding the defects, smaller area was scanned. The defects were observed like clusters, but each cluster was separated in itself. We were not able to observe both the defects and atomic resolution clearly on the same scanning area. Still it was possible to achieve atomic resolution near the defect if the defects were kept out of the scanning zone. Apparent heights of these defects were measured to be approximately 200 pm and their width was around 1 nm (see Appendix C). Apparently, STM measurement was disturbed by the defect during scanning and there was no real structural change around the defect.

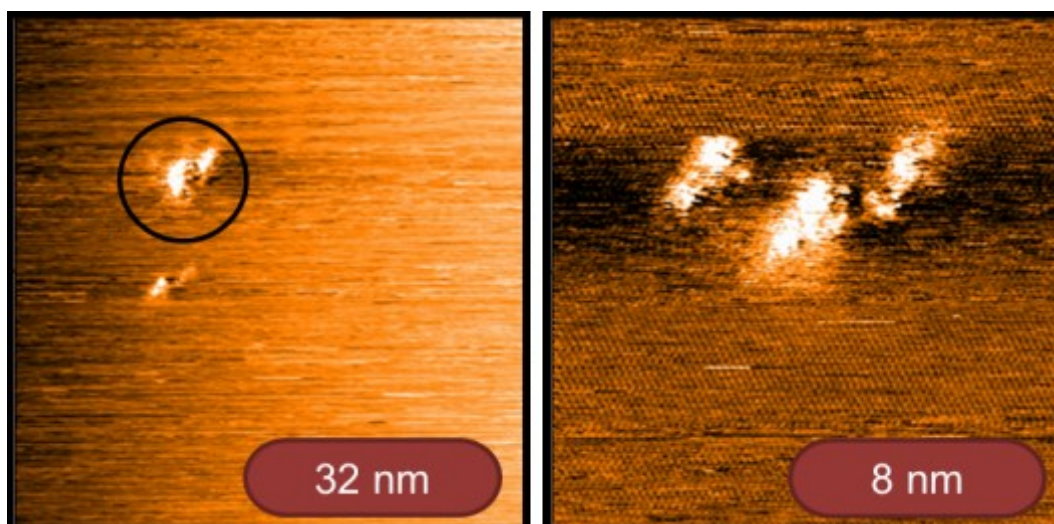


**Figure 4.2 :** STM image of defects due to the irradiation on Goodfellow-HOPG surface (left) ( $I = 0.4$  nA,  $V = -75$  mV). STM image of the defects with atomic resolution ( $I = 0.3$  nA,  $V = -100$  mV).

On different area of the same sample, we also observed single defects, which appeared different when compared to the cluster defects. Although the STM image was disturbed, atomic resolution around the defect was possible. Single defect is shown in figure 4.3 and its apparent height was measured as 100 pm. We can say that the diameter of the defect was approximately 2 nm.

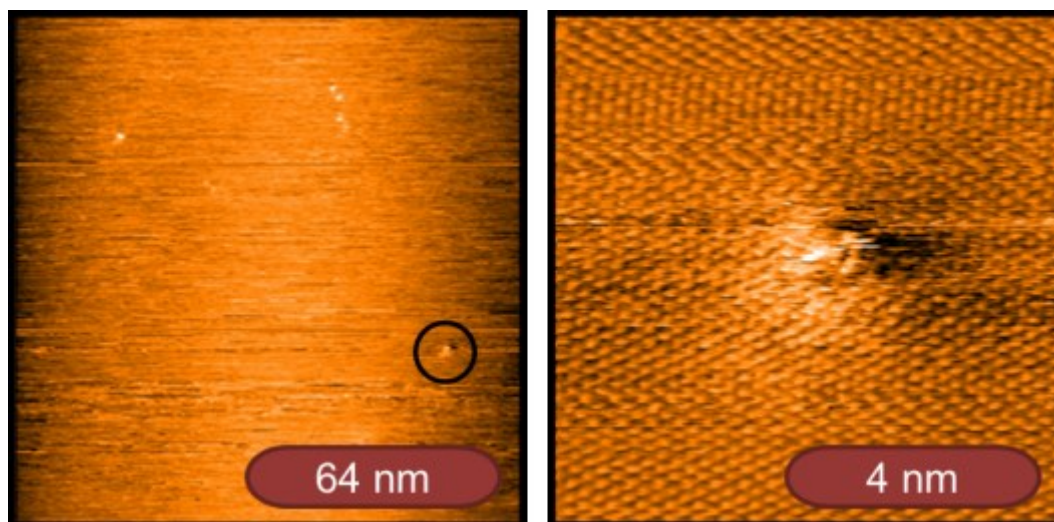


**Figure 4.3** : STM image of defects due to the irradiation, a different area (Goodfellow-HOPG surface) on the left ( $I = 0.3$  nA,  $V = -100$  mV). STM image of marked defect with atomic resolution ( $I = 0.4$  nA,  $V = -50$  mV).

Concerning the SPI-HOPG samples, cyclohexane dropcasted SPI-HOPG was chosen for the initial STM study. Since these samples were prepared for irradiation of moiré areas we first checked moiré structures. As our previous studies, we observed moiré structures on almost every tunneling zone. This means that SHI irradiation with  $^{238}\text{U}^{31+}$  ions at  $10^9$  MeV irradiation energy did not damage the general structure of moiré patterns. Defects were shown with circles on STM image in figure 4.4. Due to the flux, two defects per  $204.8 \text{ nm} \times 204.8 \text{ nm}$  are should have been counted. We counted three defects on this area.

As can be seen in figure 4.4 defects on SPI-HOPG surface were not point like even on large area so we did check the direction of the defects on moiré and clean area.



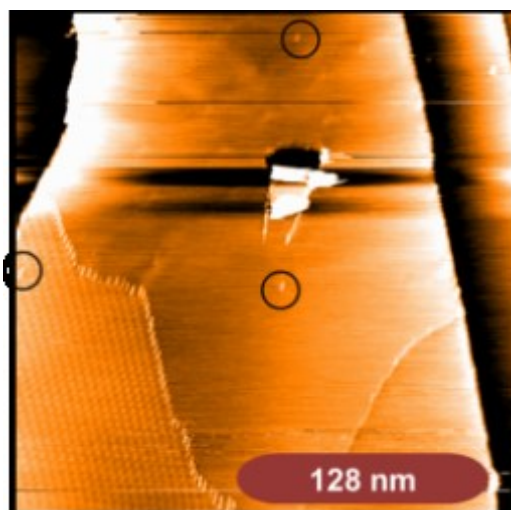


**Figure 4.4 :** Large area STM image of irradiated SPI-HOPG with moiré pattern due to dropcasted cyclohexane ( $I = 0.3$  nA,  $V = -50$  mV). Black circles show the irradiation defects.

An apparent clustering direction of the defects shown in figure 4.5, red line for the defect on moiré structure and black line for the defect on HOPG. The direction of the defects on moiré structure and HOPG part of the surface were slightly different ( $8^\circ$ ). It was possible to have such difference due to the irradiation process but structural and electronic properties of moiré patterned area and HOPG should be considered in further studies.

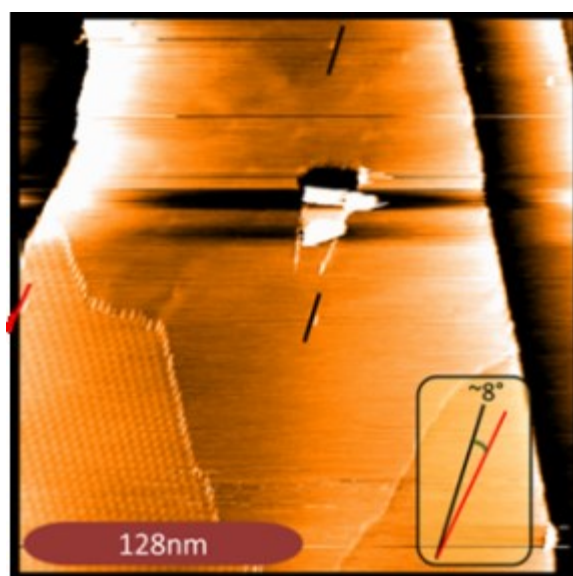


**Figure 4.5 :** STM image showing the apparent clustering direction of the defects on moiré and clean part of HOPG surface. Red line shows the direction of the defect on moiré patterned area and black lines show the direction of the defect on clean part of HOPG ( $I = 0.3$  nA,  $V = -50$  mV). The direction of the black lines were the same and angle between the directions of the red and the black lines was  $8^\circ$ .

With a closer look, the defects on SPI-HOPG was more likely triple defects (figure 4.6). Such defects can occur if the defects did not hit perpendicular to the surface (like irradiation with an angle) but perpendicular irradiation were performed on these samples. Still there was the possibility that the surface irradiated with very small angle due to the wavy structure of the surface.

Apparent height of the cluster defect was measured along the direction of three point defect and perpendicular to it. Apparent height of the structure was 152 pm. The defects were considered as three point defects on a line and width of each single point defect was measured approximately 1.6 nm along the line (total length of three defects was 5 nm). The width of the defect was measured around 2.4 nm perpendicular to the line.

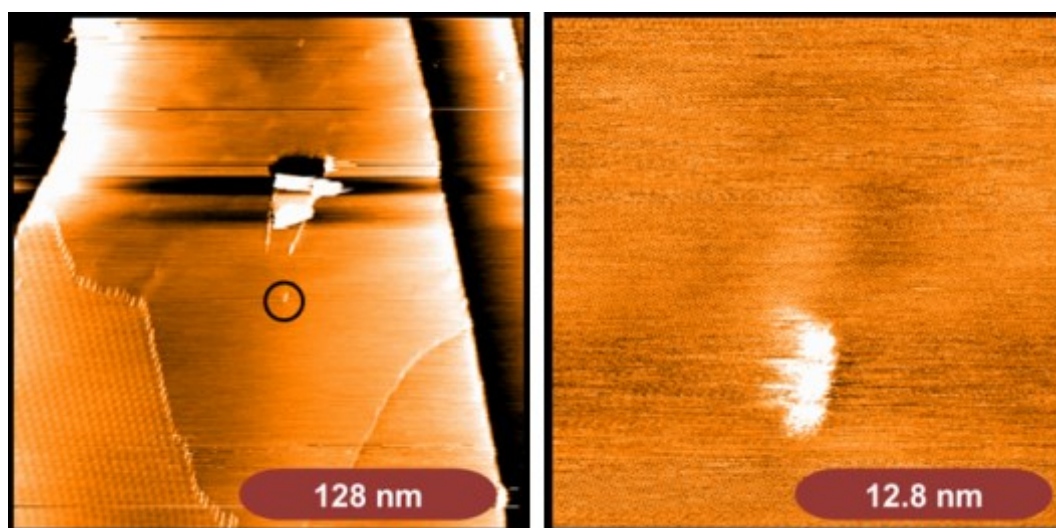


**Figure 4.6** : Zoom in STM image of SHI irradiation defect on HOPG (circle shows the defect on the left image) ( $I = 0.4$  nA,  $V = -50$  mV).

The defect on the moiré pattern was also not point like either. It was not triple defects as well. The defect was observed as it spreaded on the line. As it can be seen in figure 4.7, moiré pattern was not disturbed by the defect. Our observations on irradiated moiré structures shows that moiré spots were not individual and as stable as HOPG layer.

Apparent height of the defect on moiré structure was measured approximately 136 pm which was less than the apparent height of the defect on SPI-HOPG (it was 152 pm). Since the defect was linear, its width was measured on the line and perpendicular to it. Measured length of the defect was 5.3 nm and width of it was around 1 nm.

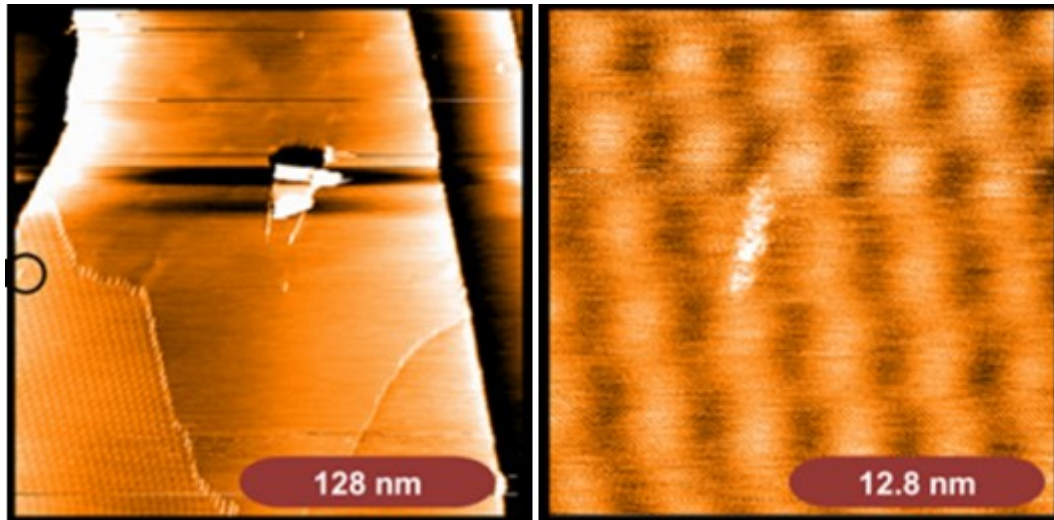


**Figure 4.7 :** Zoom in STM image of SHI irradiation defect on moiré on HOPG (circle shows the defect on the left image) ( $I = 0.4$  nA,  $V = -50$  mV).

The defects on moiré and on HOPG area were different with respect to their shape and the general nature of each defect. These two defects are shown in figure 4.8. The defect on moiré pattern was narrow and longer than the defect on the HOPG. Actually the defects on the HOPG area were like triple defects while the defect on moiré structure was spreaded on a line. Since the irradiation conditions and the source of the SHI irradiation was the same and two defects were observed on the same crystal, we can think the SHI interacted with HOPG and moiré structures differently or it can be speculated that the structure of HOPG crystals underneath each defect was locally different.

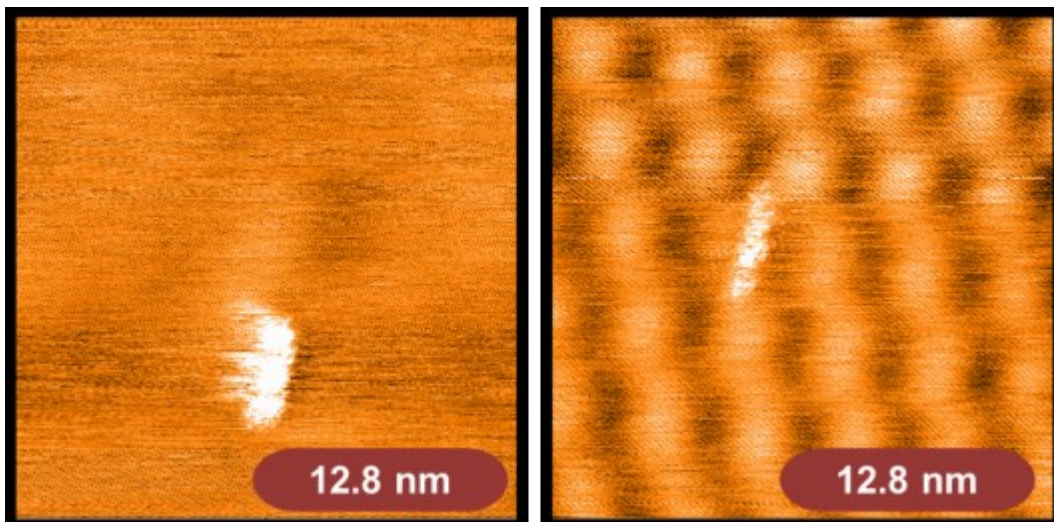


**Figure 4.8 :** STM images of irradiation defects on HOPG and on moiré ( $I = 0.4$  nA,  $V = -50$  mV).



We looked for single defects on clean area of cyclohexane dropcasted SPI-HOPG samples to compare them with the defects on Goodfellow-HOPG crystal. We found two types of single defects on SPI-HOPG so far (figure 4.9). Atomic resolution was observed on and around one of the single defects. Measured apparent height of this one was 77 pm and the width was 3 nm. However, atomic resolution near the other defect was not achieved which had higher corrugation. Apparent height of this defect was 130 pm and the width was approximately 3 nm.

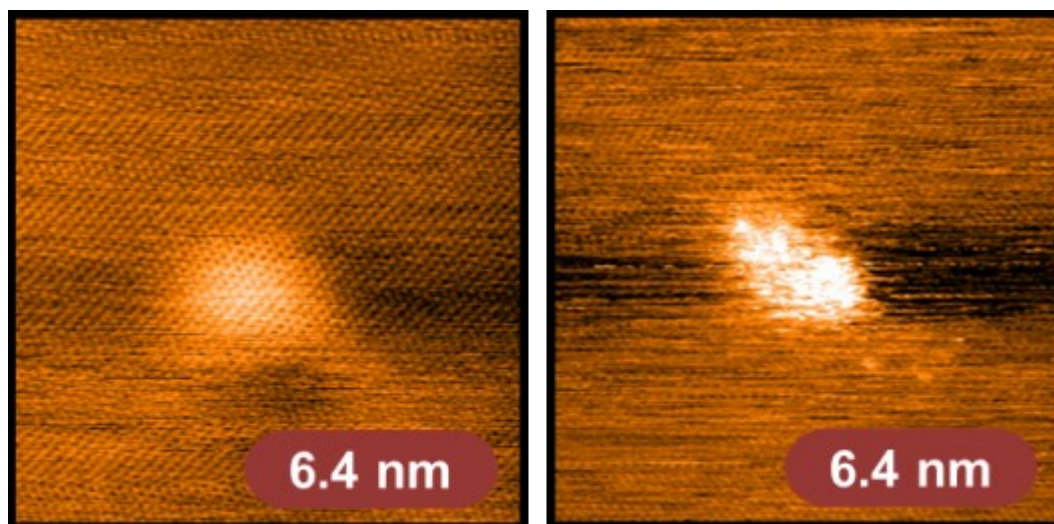


**Figure 4.9** : STM image of two different SHI irradiation defects on SPI-HOPG ( $I = 0.3$  nA,  $V = -50$  mV).

Single defects with atomic resolution and cluster defects on SPI-HOPG crystal were compared to the defects on Goodfellow-HOPG in figure-4.10.

Although single and cluster defects on HOPG crystals from different suppliers can be compared, the difference of the defects on the same crystal cannot be ignored as well. The height of the single defect on SPI-HOPG was smaller than the height of the defect on Goodfellow-HOPG. Atomic resolution was achieved around these defects.

Concerning the cluster defects, while the defects on SPI-HOPG were ordered, spreaded defects were observed on Goodfellow-HOPG surface. As a result, the defects on SPI-HOPG (both single and cluster defects) were wider and their heights were smaller compared to Goodfellow-HOPG. In addition, we were able to observe atomic resolution on or around the defect which had smaller height than 100 pm.

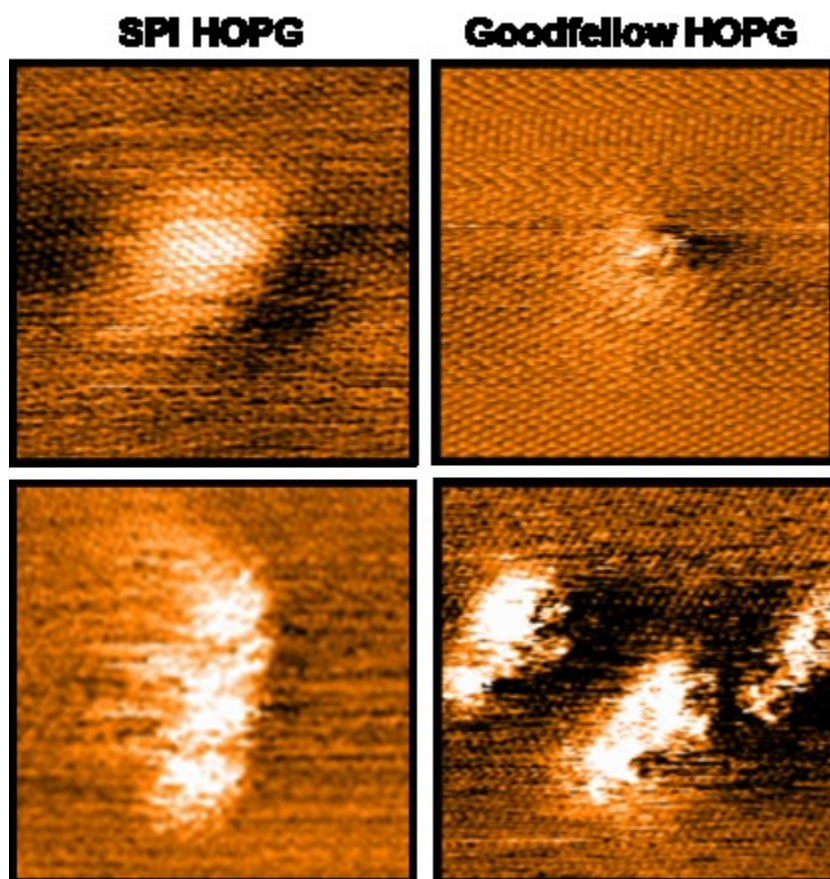


**Figure 4.10** : STM images of single ( $I = 0.3 \text{ nA}$ ,  $V = -50 \text{ mV}$ ) and cluster ( $I = 0.3 \text{ nA}$ ,  $V = -50 \text{ mV}$ ) irradiation defects on Goodfellow and SPI HOPG.

The information obtained from SHI irradiated HOPG surfaces show that not all HOPG can be compared and considered to be the same. This information in turn has a great implication on the moiré patterns forming on HOPG surfaces. There are plenty of studies on moiré patterns but none of them considers the effect of the HOPG itself and so far the reported results did not discuss the nature. With our results, we can combine both data and state that the formation of moiré patterns on HOPG surfaces due to chemicals may be a fact of the HOPG bulk itself. SHI data indicates that the encounter for the SHI with the bulk defects as it passes through may result in the structures observed at the surface. As a result we can state that, the interaction of the chemicals is a function of the crystallinity of the bulk which must be checked in further studies.

## 5. GERMANIUM(001) SURFACE

In this study, 375  $\mu\text{m}$  thick Ge wafer was cleaved and mounted on UHV-STM sample holder. Sample was prepared with degassing-annealing-sputtering-degassing-flashing cycle under UHV conditions. First results on the preparation of Ge(001) surface was proven to work positively with our STM study on Ge (001) surface. Although the surface was not entirely clean to observe Ge dimers with extreme resolution, we did observe Ge terraces and dimer rows. The STM image of Ge(001) surface as our first result with UHV-STM shown in figure 5.1. We were successful on achieving UHV conditions and sample manipulation tools were tested and they worked properly. And in the end as shown in figure-5.1 the terraces of the Ge(001) surface and the dimer rows on these terraces could be resolved.

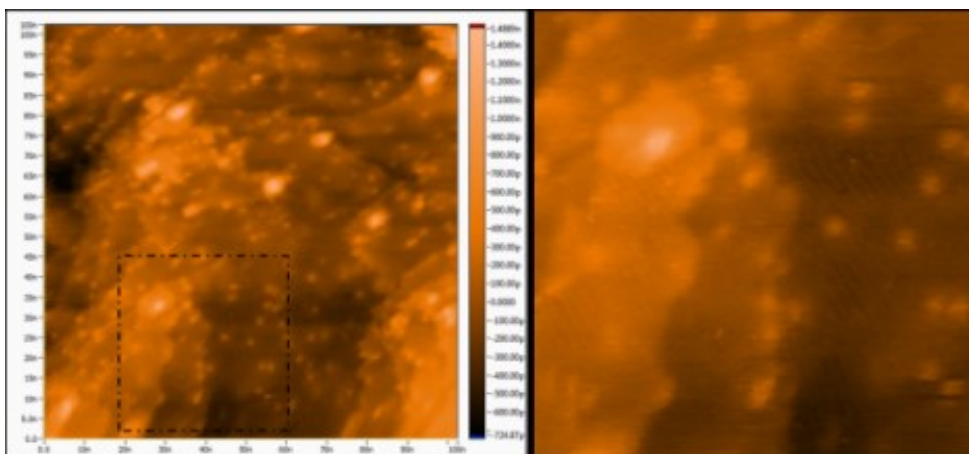


**Figure 5.1 :** STM image of Ge(001) surface with dimers. ( $I = 300\text{pA}$ ,  $V_b = -1.55\text{ V}$ ) the dimer rows on every second terrace can be seen in the left image with a 45 degree orientation with respect to the image axes.

The most important result of this part of the study is, we have proven that the UHV system is functional and UHV-STM work. More over the Ge(001) surface preparation procedure was developed from scratch in a newly constructed UHV system.



## 6. CONCLUSION AND FUTURE WORK

In this study first, the preparation method of moiré structures on HOPG surfaces were developed under ambient conditions. We found an easy and repeatable method to produce moiré structures by dropcasting cyclohexane on HOPG crystal. Besides, dropcasting cyclohexane did not damage the rest of the crystal. We did check the cyclohexane dropcasted surface with Raman spectroscopy for possible intercalation. Raman signal due to the cyclohexane was not detected from the surface.

After that, we continued with STM studies. Atomic resolution on moiré structures were achieved. Observing the atomic resolution on moiré structures at high biases was intriguing. Observing both triangular and hexagonal atomic structures on moiré patterns with a stable tip might be the result of morphological structure of these patterns.

By performing the bias depended poor man's spectroscopy on moiré structures, apparent corrugation change due to the tunneling junction bias was studied. Therefore, we showed that these structures might have different electronic states. Our contrast reversal data in comparison to a reported study supported our statement. Moreover, apparent corrugation change of moiré structures was not monotonic. Apparent corrugations were decreased with increasing absolute value of tunnel junction bias and decreasing of the apparent corrugation was not always linear. Oscillating behavior was observed on one of the moiré patterns.

Besides the experimental study on moiré structures, we did a collaborative work for theoretical calculation of these structures. Our experimental results were supported with theoretical study of Prof. Dr. Oğuz Gülseren and Dr. Şener Şen.

STS was performed on super periodic structures as well as on HOPG surface. LDOS/V curves were derived from measured I/V curves. We found that moiré patterns were more metallic than HOPG due to the LDOS/V curves. This may be the reason why STS measurements on moiré patterns are easier than on pristine HOPG surfaces. We also observed shoulders on LDOS/V curves of moiré structures, which indicate van Hove singularities. Calculated LDOS curves of these structures were consistent with our experimental results.

Our moiré study mainly shows that moiré structures have both electronic and morphological origin. Although these structures show graphene like behavior, they should be considered as different systems.

As we were aware of the difference of the HOPG crystals from different suppliers, we wanted to study on them in detail. Studying on SHI irradiation of HOPG crystals and comparing them was the continuing idea. We decided to irradiate moiré surfaces to study on SHI irradiation defects on them. It was also an opportunity to study on moiré structures from different point of view. Samples were prepared and irradiated with  $^{238}\text{U}^{+31}$  ions and studied with STM. Due to our STM measurements, moiré structures were not disturbed by the irradiation and steadily stood on HOPG surface. Although the defects were not uniform, we can safely state that formation of these defects were different depending on different HOPG suppliers. Observed defects on SPI-HOPG crystal were smaller than the defects on Goodfellow-HOPG.

Construction of the UHV system was a time consuming work in this thesis study. We did design and construct a vibration isolation table for the system. We did construct the UHV system on that table. Sample manipulator and other parts were modified to heat the sample. Sample carrier was made to put spare samples into the UHV chamber. For further studies, Pt evaporator was made on a feedthrough. All these parts and UHV-STM were tested under UHV as we achieved pressures less than  $5 \times 10^{-10}$  mbar. Ge(001) crystal was prepared under UHV conditions and dimer rows were observed by UHV-STM. Observing dimer rows shows that UHV conditions were achieved and sample preparation procedure was successfully developed during this study under UHV conditions.

During this study several different physical systems were looked at and some required experimental procedures were developed. Consequently this work generated many probable future study opportunities.

Moiré patterns will be studied with atomic force microscope (AFM) and kelvin probe force microscope (KPFM) as a continuing study.  $dI/dV$  maps will be generated on these structures under ambient conditions.

We will continue STM study of SHI irradiation defects on HOPG (SPI and Goodfellow) and moiré structures. More defects will be observed to compare them due to the crystals. Atomic resolution will be achieved on single defects. Single defects will be searched on moiré structures. Atomic resolution will be achieved on or around the defects on moiré structures. STS will be performed on and around the defects especially on moiré patterns. In addition, we will investigate the defect

formation on HOPG crystals that were irradiated with an angle. With this data we intend to understand the defect formation in HOPG due to SHI irradiation.

Preparation procedure will be improved for Ge(001) surface. Ge dimers will be observed by using STM. We will evaporate Pt on Ge(001) surface and we will prepare metallic nanowires. We will do STM and STS study on the wires and we will try atomic manipulation at room temperature.





## REFERENCES

- [1] **Wallace P. R.** (1947). The Band Theory of Graphite *Physical Review Letters*
- [2] **Tomanek, D., Louie, S. G., Mamin, H. J., Abraham, D. W., Thomson, R. E., Ganz, E., Clarke, J.** (1987). Theory and observation of highly asymmetric atomic structure in scanning-tunneling-microscopy images of graphite, *Phys. Rev. B.* 35, 7790.
- [3] **Chen, C. J.** (1993). *Introduction to Scanning Tunneling Microscopy*. New York: Oxford University Press.
- [4] **Venables, J. A.** (2001). *Introduction to Surface and Thin Film Processes*. Cambridge: University Press.
- [5] **Url-1** <[http://en.wikipedia.org/wiki/Moir%C3%A9\\_pattern](http://en.wikipedia.org/wiki/Moir%C3%A9_pattern)>, data retrieved 15.12.2013.
- [6] **Wang Y., Ye Y., Wu K.** (2006). Simultaneous observation of the triangular and honeycomb structures on highly oriented pyrolytic graphite at room temperature: An STM study, *Surface Science* 600, p.729
- [7] **Beyer H., Müller M., Schimmel T.** (1999). Monolayers of Graphite Rotated By A Defined Angle: Hexagonal Superstructures by STM, *Appl. Phys. A* 68, p.163.
- [8] **Cao G., Zhang J.** (2005) STM Study of Moiré Patterns on HOPG, *Chin. J. Chem. Phys.* Vol.19, No. 3, p.197.
- [9] **Xhie J., Sattler K., Ge M., Venkateswaran N.** (1993). Giant and Supergiant Lattices On Graphite, *Phys. Rev. B* 47, p.15835
- [10] **Bernhardt T.M., Kaiser B., Rademann K.** (1998). Formation of Superperiodic Patterns on Highly Oriented Pyrolytic Graphite by Manipulation of Nanosized Graphite Sheets With The STM Tip, *Surface Science* 408, p.86.
- [11] **K. Miyake et al.**, (1998) Giant Superstructures Formed On Graphite Surface Treated with NaOH Solutions Studied by Scanning Tunneling Microscopy, *Ultramicroscopy* 73, 185.
- [12] **Kuwabara, M., Clarke, D.R., Smith, D. A.** (1990). Anomalous superperiodicity in scanning tunneling microscope images of graphite, *Appl. Phys. Lett.* 56 (24).
- [13] **Cisternas, E., Flores, M., Vargas P.** (2008). Superstructures in arrays of rotated graphene layers: Electronic structure calculations, *Phys. Rev. B.* 78, 125406.
- [14] **Xhie, J., Sattler, K., Ge, M., Venkateswaran, N.** (1993) Giant and supergiant lattices on graphite, *Physical Review B* 47, 23.
- [15] **A. H. Castro Neto, F. G.** (2009). The electronic properties of graphene. *Reviews Of Modern Physics*, 81.

- [16] **A. Luican, I. G.** (2011). Single-Layer Behavior and Its Breakdown in Twisted Graphene Layers. *PHYSICAL REVIEW LETTERS*, 106(26802).
- [17] **B. FEDDES, I. K.** (1998). On Superperiodic Features on Highly Oriented Pyrolytic Graphite. *SCANNING*, 20, 376-379.
- [18] **David L. Miller, K. D.** (2010). Structural analysis of multilayer graphene via atomic moiré interferometry. *PHYSICAL REVIEW B*, 81(125427).
- [19] **Durkan, H. S.** (2010). Unraveling the rotational disorder of graphene layers in graphite. *PHYSICAL REVIEW B*, 81(045403).
- [20] **Durkan, H. S.** (2011). Imaging confined charge density oscillations on graphite at room temperature. *PHYSICAL REVIEW B*, 84(085435).
- [21] **E. Cisternas, F. S.** (2009). First-principles calculation and scanning tunneling microscopy study of highly oriented pyrolytic graphite (0001). *PHYSICAL REVIEW B*, 79(205431).
- [22] **H. Beyer, M. M.** (1999). Monolayers of graphite rotated by a defined angle: hexagonal superstructures by STM. *Appl. Phys. A*, 68, 163–166.
- [23] **Hai-Lin Sun \*, Q. T. S. F. Z. K.** (2003). Scanning tunneling microscopy study of superlattice domain boundaries on graphite surface. *Surface Science*, 542, 94–100.
- [24] **Hong Seng Wong, C. D.** (2009). Tailoring the Local Interaction between Graphene Layers in Graphite at the Atomic Scale and Above Using Scanning Tunneling Microscopy. *ACS NANO*, 3(11), 3455–3462.
- [25] **J. M. Campanera, G. M.** (2007). Density functional calculations on the intricacies of Moiré patterns on graphite. *PHYSICAL REVIEW B*, 75(235449).
- [26] **J. Osing, I. S.** (1998). Bulk defects in graphite observed with a scanning tunnelling microscope. *Surface Science*, 417, 145–150.
- [27] **J. Xhie, K. S.** (1993). Giant and supergiant lattices on graphite. 47(23).
- [28] **K. Miyake, K. A.** (1998). Giant superstructures formed on graphite surface treated with. *Ultramicroscopy*, 73, 185-189.
- [29] **Kobayashi, K.** (1995). Moire pattern in scanning tunneling microscopy: Mechanism in observation. *PHYSICAL REVIEW B*, 53(16).
- [30] **Kuiper, Z. Y.** (1993). Electronic effects in scanning Moire on a microscopy: surface. *PHYSICAL REVIEW B*, 48(23).
- [31] **Ouseph, P. J.** (1996). Transformation of a graphite superlattice into triangular dislocations. *PHYSICAL REVIEW B*, 53(15).
- [32] **P. Xu, Y. Y.-L.** (2011). Giant surface charge density of graphene resolved from scanning tunneling microscopy. *PHYSICAL REVIEW B*, 84(161409(R)).

- [33] **Rong, Z. Y.** (1964). Extended modifications of electronic structures caused by defects: Scanning tunneling microscopy of graphite. *PHYSICAL REVIEW B*, 50(3).
- [34] **T.M. Bernhardt, B. K.** (1998). Formation of superperiodic patterns on highly oriented pyrolytic graphite by manipulation of nanosized graphite sheets with the STM tip. *Surface Science*, 408, 86-94.
- [35] **Yang Gan, W. C.** (2003). STM investigation on interaction between superstructure and grain boundary in graphite. *Surface Science*, 539, 120–128.
- [36] **Yongfeng Wang, Y. Y.** (2006). Simultaneous observation of the triangular and honeycomb structures on highly oriented pyrolytic graphite at room temperature: An STM study. *Surface Science*, 600, 729-736.
- [37] **Pong W.T, Durkan C.** (2005). A Review And Outlook For An Anomaly Of Scanning Tunneling Microscopy (STM): Superlattices On Graphite, *J. Phys. D: Appl. Phys.* Vol.38, R329.
- [38] **Johann Coraux, A. T.-J.** (2009). Growth of graphene on Ir(111). *New Journal of Physics*, 11.
- [39] **E. N. Voloshina<sup>1</sup>, E. F.** (2013). Electronic structure and imaging contrast of graphene moiré on metals. *SCIENTIFIC REPORTS*.
- [40] **J. Liu, C. T.** (2002). Graphite irradiated by swift heavy ions under grazing incidence. *Nuclear Instruments and Methods in Physics Research B*, 193, 259–264.
- [41] **J. Liu, M. H.** (2003). STM and Raman spectroscopic study of graphite irradiated by heavy ions. *Nuclear Instruments and Methods in Physics Research B*, 212, 303–307.
- [42] **J. Liu, R. N.** (2001). Tracks of swift heavy ions in graphite studied by scanning tunneling microscopy. *Phys. Rev. B*, 64(184115).
- [43] **Oguzhan Gurlu, H. J.** (2004). Electronic Properties of (2×1) and c(4×2) Domains on Ge(001) Studied by Scanning Tunneling Spectroscopy. *Physical Review Letters*, 93(066101).
- [44] **Oguzhan Gurlu, O. A.** (2003). Self-organized, one-dimensional Pt nanowires on Ge(001). *Applied Physics Letters*, 83 (22).
- [45] **G. Binnig, H. R.** (1983). 7 × 7 Reconstruction on Si(111) Resolved in Real Space. *Physical Review Letters*, 50(120).
- [46] **Url-2** <<http://www.ganil-spiral2.eu/>>, data retrieved 25.04.2014.



## **APPENDICES**

**APPENDIX A:** Approach mechanism of UHV-STM

**APPENDIX B:** Theoretical study on moiré structures.

**APPENDIX C:** Height profiles of irradiation defects on HOPG and moiré structures.

## APPENDIX A

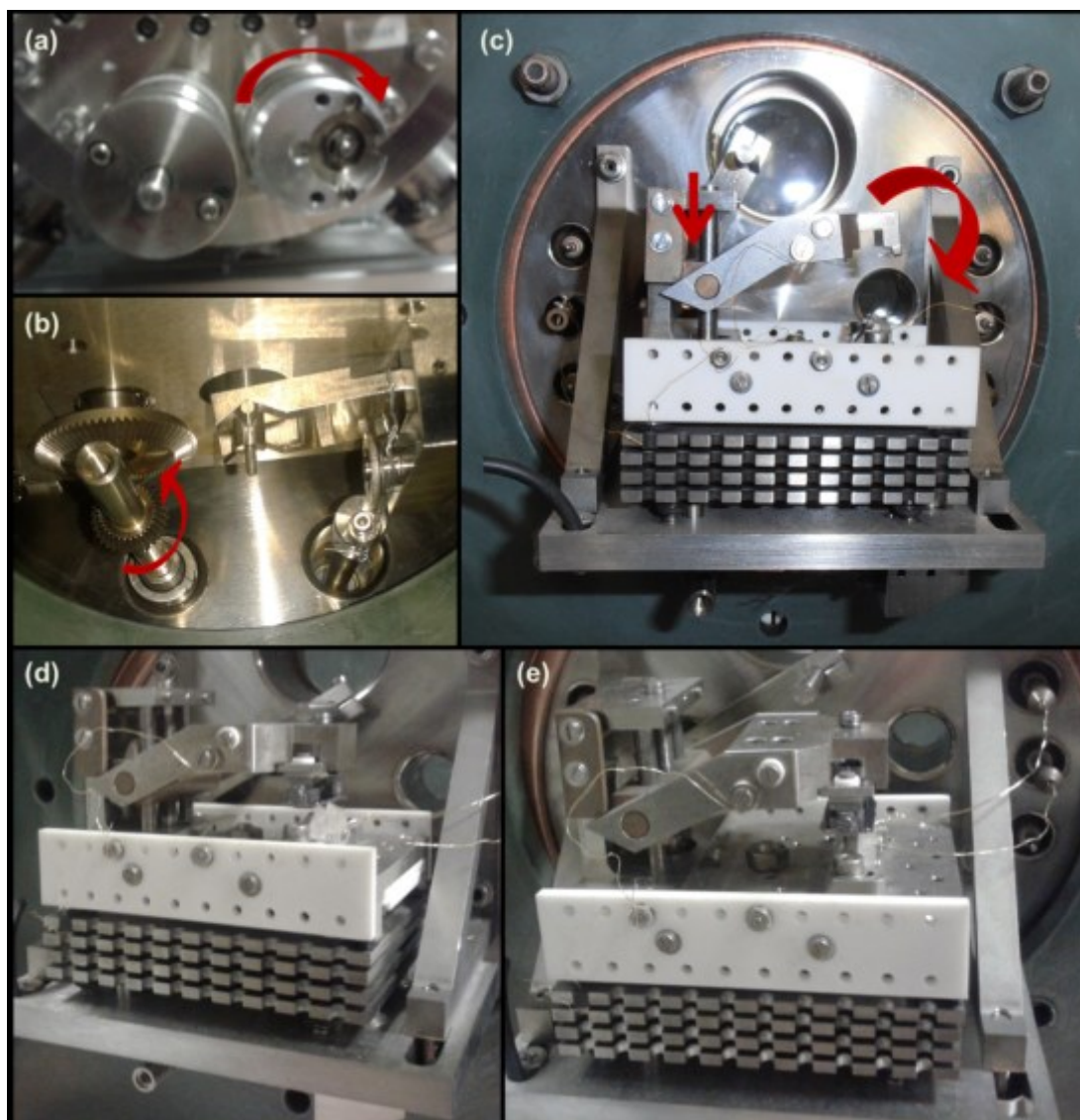


**Figure A.1** : Approach mechanism of UHV-STM. By using the rotational feedthrough (a) worm gear (b) is rotated. Sample is approached by rotated worm gear. (d) & (e) sample approached.

## APPENDIX B

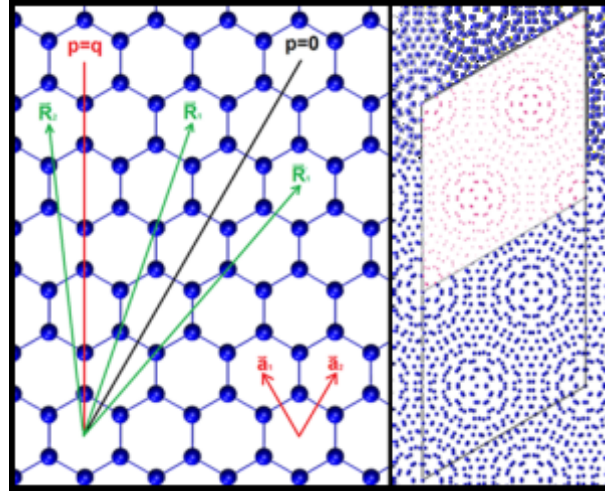


**Figure B.1 :** Generation of moiré pattern (left). Generated moiré pattern, inset image shows calculated charges for this pattern.

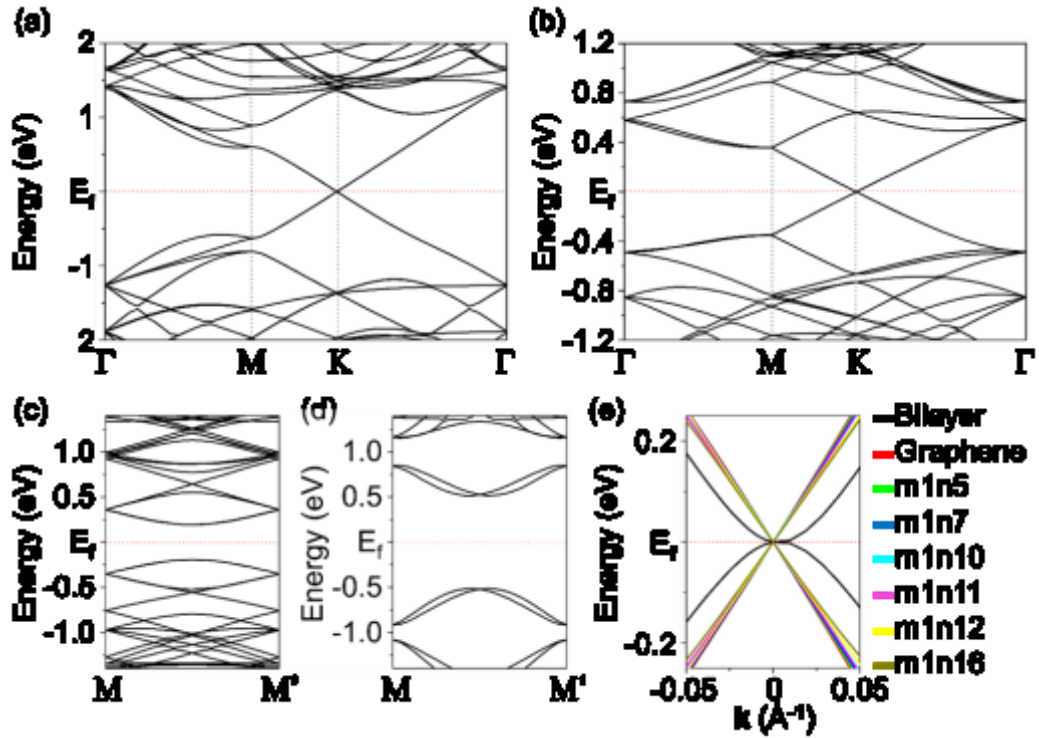


**Figure B.2 :** Calculated band structure of (a) m1n10 moiré structure, (b) m1m12 moiré structure with ab initio. Calculated band structure of (c) m1n11 moiré structure (d) m1n7 moiré structure between high symmetry points M and M'. (e) Band dispersion around high symmetry point K for various systems which exhibits linear and second order behaviour.



## APPENDIX C

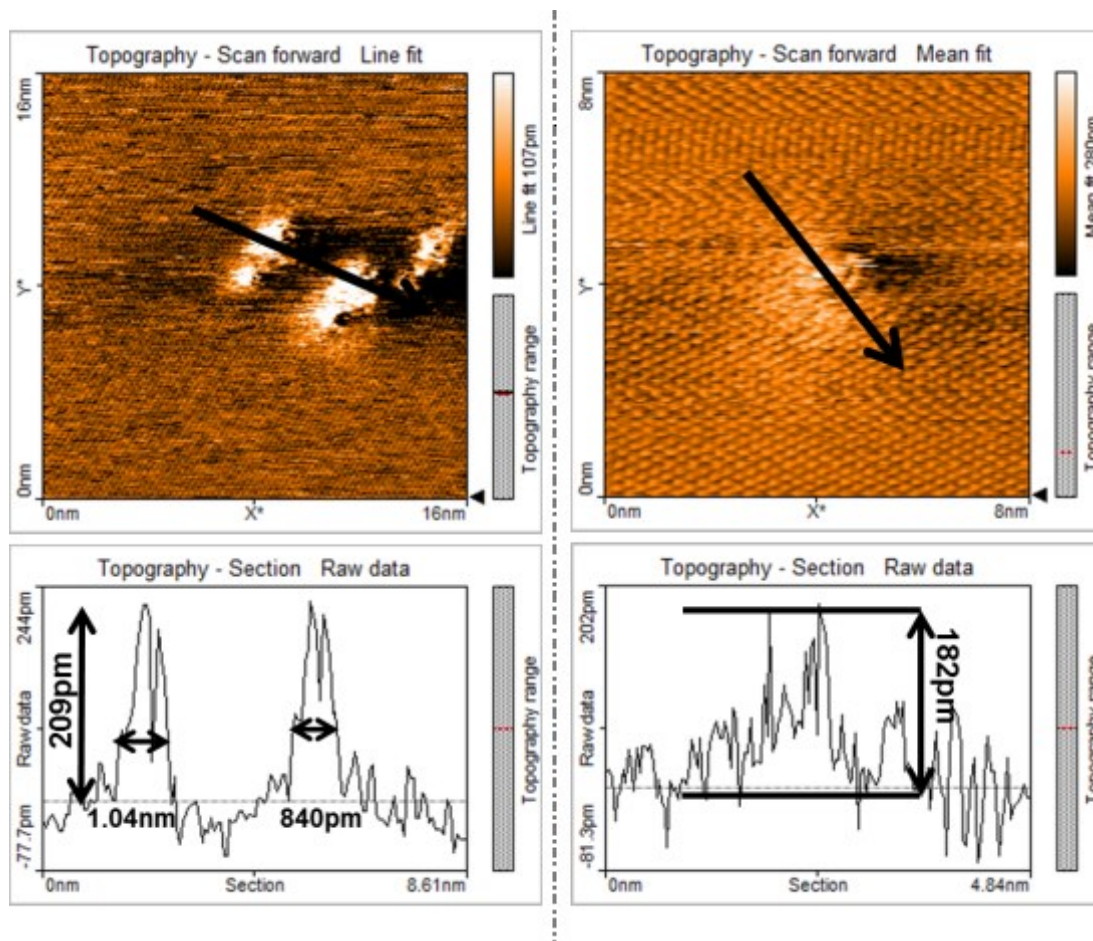


**Figure C.1 :** Height profiles of irradiation defects on GF-HOPG. (a) triple defects (b) single defect.

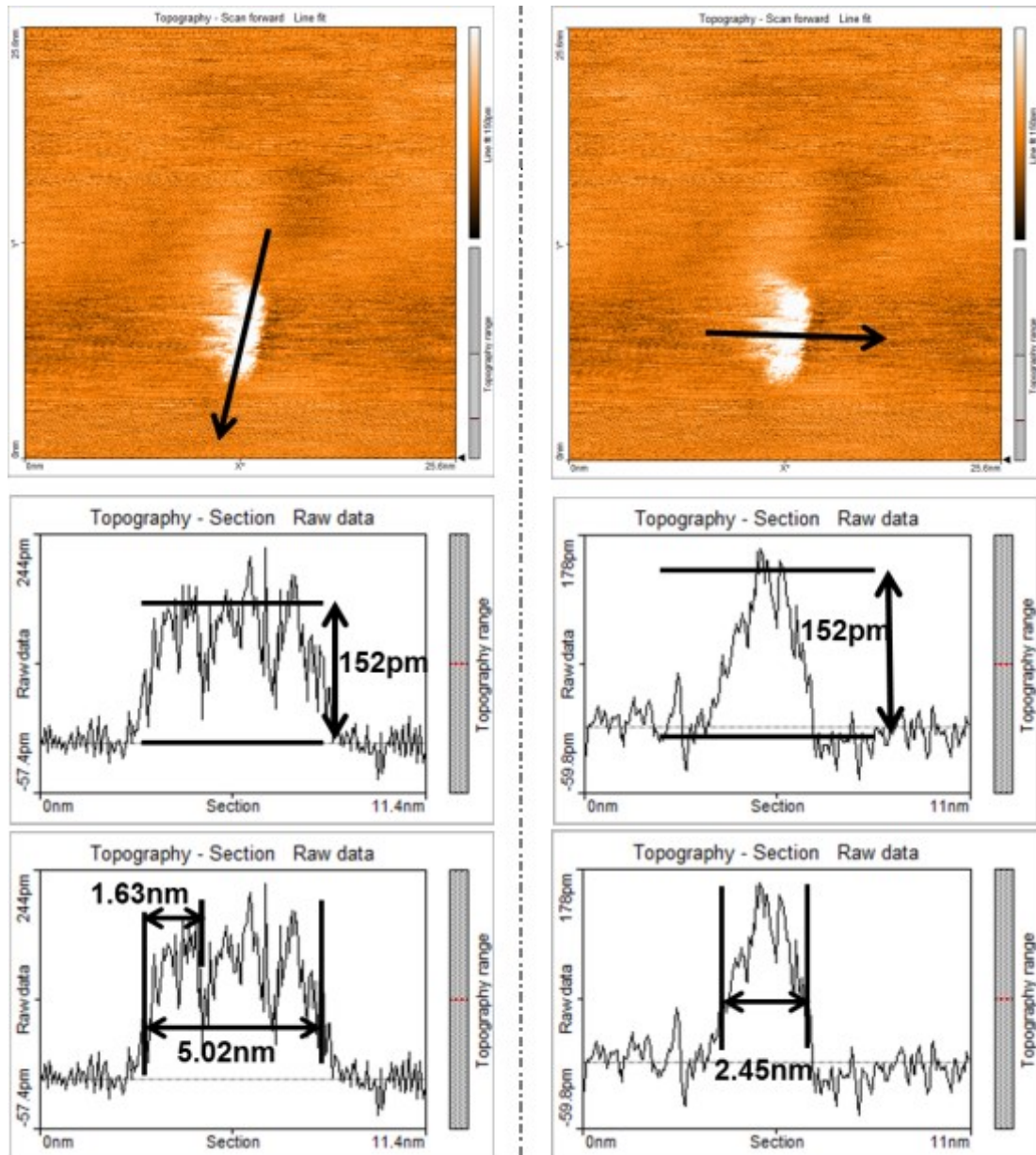


**Figure C.2 :** Height profiles of irradiation defects on SPI-HOPG. The defects on HOPG part were like triple defect on a line. It was not multiple separated point defects but spreaded defect on a line. Unlike the multiple defects on Goodfellow HOPG, the multiple defects on SPI HOPG were ordered. The height of the multiple defects on SPI HOPG was lower and width of them was wider. Still atomic resolution on or around the defect was not observed.

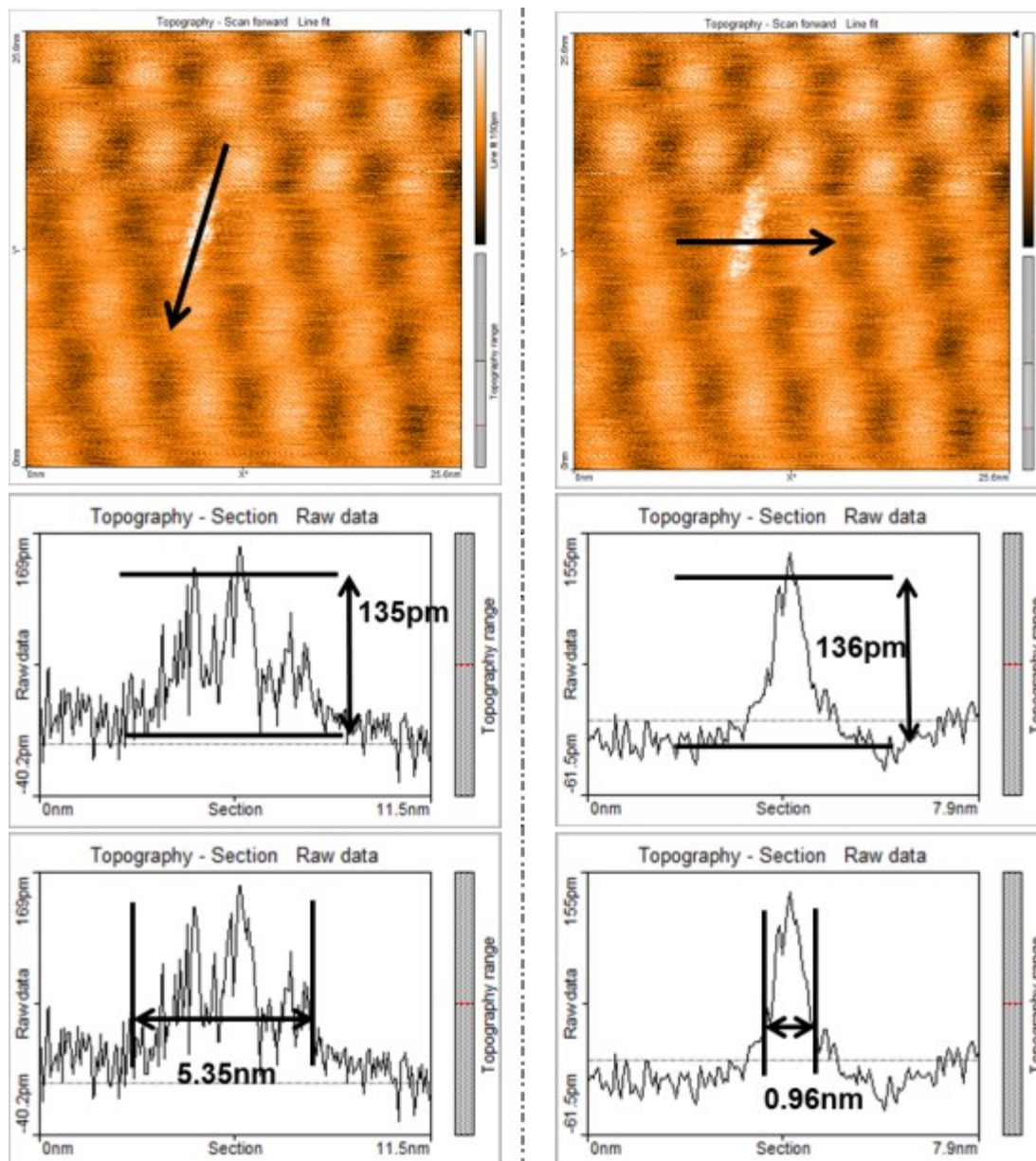


**Figure C.3 :** Height profiles of irradiation defects on moiré structures on SPI-HOPG. Unlike the defect on HOPG part, the defect on moiré pattern was like a line defect. It was not multiple separated point defects but spreaded defect on a line. Clearly, the defect on moiré pattern was more narrow and longer. Atomic resolution on or around the defect was not observed. Still defect formations were different on moiré pattern and HOPG.



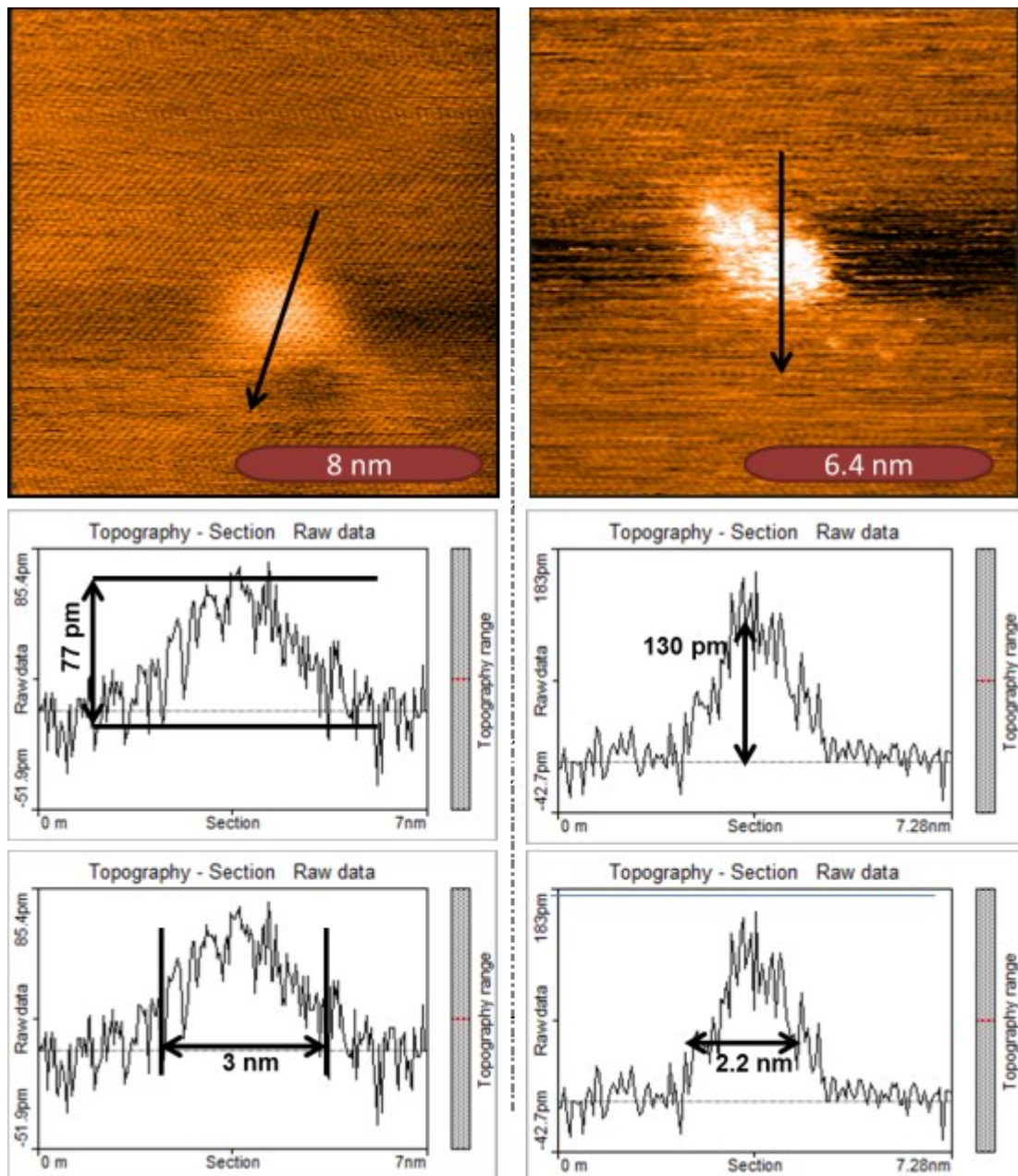


**Figure C.4 :** Height profile of single defects on SPI-HOPG. Atomic resolution on the defect was observed on single irradiation defect on SPI-HOPG (left). The apparent height of this defect was measured as 77 pm. Apparent height of the defect on the right was 130 pm and it was not possible to achieve atomic resolution on the defect. It is possible that achieving atomic resolution on or around the defect depends on the height of the defect.

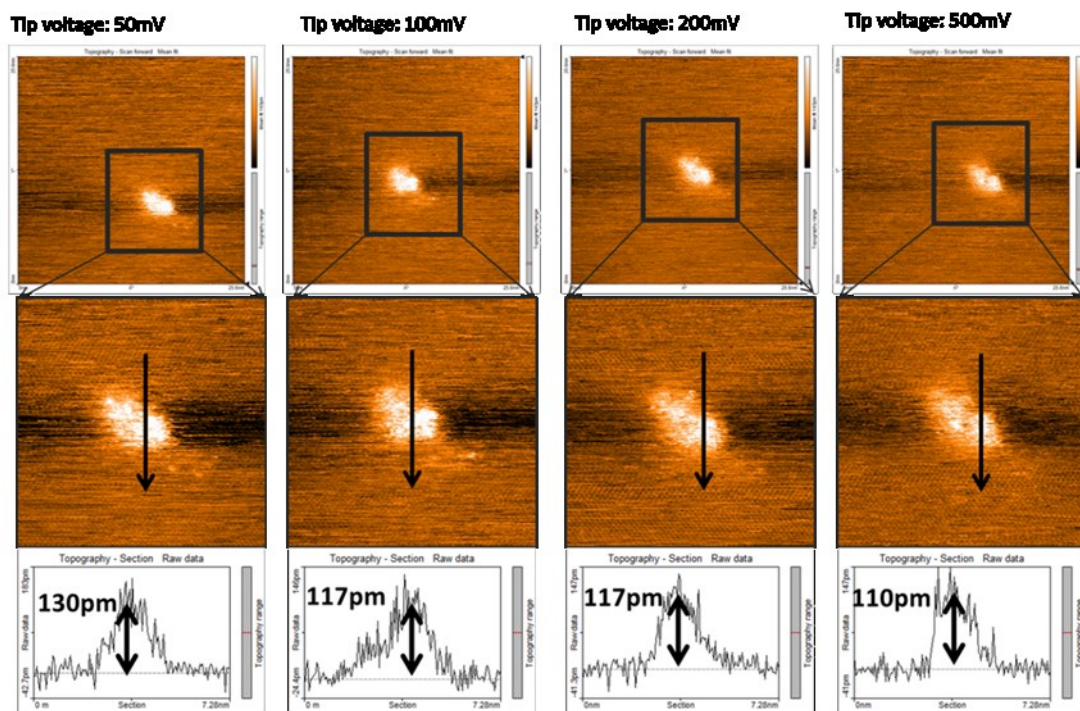


**Figure C.5 :** Bias dependent height profile on single defect on SPI HOPG. Heights of the defects decrease with increasing tip bias. Although atomic reconstruction were not observed on irradiated HOPG surfaces, changing of the apparent heights of the defects show that irradiation defects change the electronic properties of HOPG.

## **CURRICULUM VITAE**



**Name Surname:** Dilek YILDIZ

**Place and Date of Birth:** Orhaneli 22.01.1988

**E-Mail:** yildizdi@itu.edu.tr

**B.Sc.:** İstanbul Technical University  
Physics Engineering

### **Professional Experience and Rewards:**

Engineering Workshop Internship at Mechanical Engineering Faculty, ITU (4 weeks, summer 2008): Turning machine, milling machine, planning machine, and welding (basic training).

Laboratory internship, Faculty of Science and Letters, ITU (10 weeks, summer 2010): Design and construction of vibration isolation system for UHV-STM system.

Laboratory internship, Faculty of Science, Bilkent University, Ankara, Turkey (4 weeks, summer 2010): Optic lithography for making graphene devices.

Nanoelectronic and Nanophotonics Winter School, Bilkent, Ankara (20-25 Jan 2009)

Physics and Chemistry of Solids: Theory and Experiment Winter School, Bilkent, Ankara (6-12 Nov 2011)

Manager and researcher in one-year undergrad project (supported by TÜBİTAK BİDEB-2209): Preparation and Investigation of Moire patterns on Graphene/HOPG system with Scanning Tunneling Microscopy (STM) and Spectroscopy (STS).

Research Assistant in TÜBİTAK 1001 project (project number: 109T687 – 9 months): Observation of Optical Excitations at Nano Size Tunneling Junction (by means of Photon STM).

Research Assistant in TÜBİTAK 1001 project (project number: 112T818 – 4 months): Formation and Investigation of the Physical Properties of Metallic Nanowires on Semiconductor Surfaces and their Manipulation.

Research Assistant in TÜBİTAK- CNRS joint - project (project number: 113F005 –10 months): Investigation of Morphological and Electronic Properties of Graphitic Surfaces Bombarded with Swift Heavy Ions.

Best poster prize in NANO-TR7 (7th National Nanoscience and Nanotechnology Conference): Morphological and Electronic Properties of Super Periodic Structures Due To Graphene Layers on HOPG Surfaces

#### **List of Publications and Patents:**

##### **PUBLICATIONS/PRESENTATIONS ON THE THESIS**

- Yıldız D.**, Erdoğan E., Gürlü O., 2009: Moire Structures on Graphene/HOPG system. *ITU Nano-Science and Nano-Technology Workshop - ITU, Istanbul.*
- Yıldız D.**, Ersoy E., Gürlü O., 2010: Morphological and electronic properties of Moire patterns on graphene and graphitic layers on HOPG. *NANO-TR6 (6th National Nanoscience and Nanotechnology Conference) - IYTE, Izmir.*
- Yıldız D.**, Şen Ş., Gülseren O., Gürlü O., 2011: Morphological and Electronic Properties of Super Periodic Structures Due To Graphene Layers on HOPG Surfaces. *NANO-TR7 (7th National Nanoscience and Nanotechnology Conference) - Sabanci University, Istanbul*
- Yıldız D.**, Şen Ş., Gülseren O., Gürlü O., 2012: Electronic properties of super-periodic structures due to dislocated graphene on HOPG. *ECOSS-29 (29th European Conference on Surface Science) - Edinburgh, UK.*
- Gürlü O., Tamer M. S., Sertkol M., Yılmaz R., **Yıldız D.**, 2012: Photon scanning tunneling microscopy of alloyed gold surfaces. *ECOSS-29 (29th European Conference on Surface Science) - Edinburgh, UK.*
- Yıldız D.**, Şen Ş., Gülseren O., Gürlü O., 2013: Morphological and Electronic Study of Moirè Patterns due to Dislocated Graphene on HOPG. *DPG Spring Meeting of the Condensed Matter Section - Regensburg, Germany*